geodiversitas

2021 • 43 • 7

New material of the frog *Hungarobatrachus szukacsi* Szentesi & Venczel, 2010 from the Santonian of Hungary, supports its neobatrachian affinities and reveals a Gondwanan influence on the European Late Cretaceous anuran fauna

Márton VENCZEL, Zoltán SZENTESI & James D. GARDNER

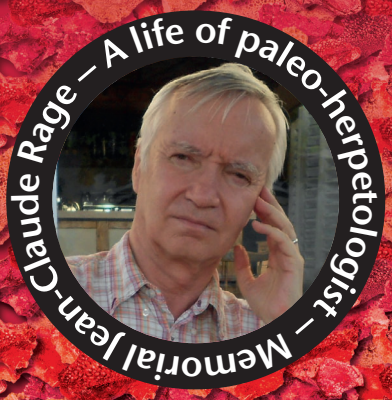

art. 43 (7) — Published on 8 April 2021
www.geodiversitas.com

PUBLICATIONS SCIENTIFIQUES

MUSÉUM NAL HIST NATURELLE

Geodiversitas est indexé dans / Geodiversitas *is indexed in:*
– Science Citation Index Expanded (SciSearch®)
– ISI Alerting Services®
– Current Contents® / Physical, Chemical, and Earth Sciences®
– Scopus®

Geodiversitas est distribué en version électronique par / Geodiversitas *is distributed electronically by:*
– BioOne® (http://www.bioone.org)

Les articles ainsi que les nouveautés nomenclaturales publiés dans *Geodiversitas* sont référencés par / *Articles and nomenclatural novelties published in* Geodiversitas *are referenced by:*
– ZooBank® (http://zoobank.org)

Geodiversitas est une revue en flux continu publiée par les Publications scientifiques du Muséum, Paris
Geodiversitas *is a fast track journal published by the Museum Science Press, Paris*

Les Publications scientifiques du Muséum publient aussi / *The Museum Science Press also publish:* ***Adansonia***, ***Zoosystema***, ***Anthropozoologica***, ***European Journal of Taxonomy***, ***Naturae***, ***Cryptogamie*** **sous-sections** ***Algologie***, ***Bryologie***, ***Mycologie, Comptes Rendus Palevol***

Diffusion – Publications scientifiques Muséum national d'Histoire naturelle
CP 41 – 57 rue Cuvier F-75231 Paris cedex 05 (France)
Tél. : 33 (0)1 40 79 48 05 / Fax : 33 (0)1 40 79 38 40
diff.pub@mnhn.fr / http://sciencepress.mnhn.fr

ISSN (imprimé / *print*) : 1280-9659/ ISSN (électronique / *electronic*) : 1638-9395

New material of the frog *Hungarobatrachus szukacsi* Szentesi & Venczel, 2010, from the Santonian of Hungary, supports its neobatrachian affinities and reveals a Gondwanan influence on the European Late Cretaceous anuran fauna

Márton VENCZEL
Department of Natural History, Ţării Crişurilor Museum,
Dacia Ave. 1-3, 410464 Oradea, (Romania)
mvenczel@gmail.com (corresponding author)

Zoltán SZENTESI
Department of Palaeontology and Geology, Hungarian Natural History Museum,
1088 Budapest, Pf. 137 (Hungary)
szentesi.zoltan@nhmus.hu

James D. GARDNER
Royal Tyrrell Museum of Palaeontology, Box 7500, Drumheller, Alberta T0J 0Y0 (Canada)
james.gardner@gov.ab.ca

Submitted on 12 September 2019 | accepted on 10 December 2019 | published on 8 April 2021

urn:lsid:zoobank.org:pub:74E9AB7F-BE18-428A-BB93-FE8B79AFC455

Venczel M., Szentesi Z. & Gardner J. D. 2021. — New material of the frog *Hungarobatrachus szukacsi* Szentesi & Venczel, 2010, from the Santonian of Hungary, supports its neobatrachian affinities and reveals a Gondwanan influence on the European Late Cretaceous anuran fauna, *in* Steyer J.-S., Augé M. L. & Métais G. (eds), Memorial Jean-Claude Rage: A life of paleo-herpetologist. *Geodiversitas* 43 (7): 187-207. https://doi.org/10.5252/geodiversitas2021v43a7. http://geodiversitas.com/43/7

ABSTRACT
The Late Cretaceous anuran *Hungarobatrachus szukacsi* Szentesi & Venczel, 2010 was erected for isolated ilia and tibio-fibulae from the Santonian-age Iharkút locality, in northwestern Hungary. On the strength of ilial features, *H. szukacsi* was interpreted as a neobatrachian and possible ranoid, making it the only pre-Cenozoic occurrence for both clades in Laurasia. New ilia and the first examples of skull bones (incomplete frontoparietals, squamosals, maxillae, and angulosplenials) from the type locality provide new insights into the taxonomic distinctiveness, osteology, and evolutionary history of *H. szukacsi*. In addition to its diagnostic ilia (e.g., dorsal crest tall and ornamented laterally with prominent ridges; extensive interiliac tubercle developed across entire medial surface of acetabular region), *H. szukacsi* is characterized further by having a moderately hyperossified skull exhibiting such traits as frontoparietals, squamosals, and maxillae externally covered with prominent pit-and-ridge and weakly developed tuberculate ornament (i.e., exostosis), frontoparietals solidly fused along midline, frontoparietals expanded posterolaterally to form a broad squamosal process, squamosals expanded anteroposteriorly to form a plate-like lamella alaris, and maxilla articulating posteriorly with the quadratojugal to form a solid bony 'cheek'. The first cladistic analysis to include *H. szukacsi* corroborates its neobatrachian status, but consistently places it among hyloids, rather than ranoids as originally proposed. Indications of hyloids on the African continent and in Madagascar during the Late Cretaceous, suggest that the ancestor of *H. szukacsi* may have dispersed from Africa, across the proto-Mediterranean and into Europe, prior to the Santonian.

KEY WORDS
Apulian microplate,
Gondwana,
Neobatrachia,
Hyloides,
palaeogeography.

RÉSUMÉ
Un nouveau matériel de la grenouille Hungarobatrachus szukacsi *Szentesi & Venczel, 2010 du Santonien de Hongrie confirme ses affinités néobatrachiennes et révèle une influence gondwanienne sur la faune d'anoures du Crétacé supérieur européen.*
Hungarobatrachus szukacsi Szentesi & Venczel, 2010, anoure du Crétacé supérieur du nord-ouest de Hongrie, a été érigé à partir d'ilions et de tibio-fibulae isolés de la localité d'Iharkút (Santonien). Sur la base de caractères de l'ilion, *H. szukacsi* a été interprété comme un Neobatrachia, peut-être ranoïde, ce qui en fait la seule occurrence pré-cénozoïque de ces deux clades en Laurasie. De nouveaux ilions et les premiers exemples d'os du crâne (frontopariétaux, squamosaux, maxillaires et angulospléniaux, tous incomplets) provenant de la localité type fournissent de nouvelles informations sur la spécificité taxonomique, l'ostéologie et l'histoire évolutive de *H. szukacsi*. En plus de ses ilions diagnostiques (présentant par exemple une crête dorsale haute et ornementée latéralement avec des crêtes proéminentes et un tubercule interiliaque étendu et développé sur toute la surface médiale de sa région acétabulaire), *H. szukacsi* est caractérisé en outre par un crâne assez hyperossifié avec des frontopariétaux, des squamosals et des maxillaires recouverts extérieurement d'une ornementation de type « pit and ridge » avec des tubercules faiblement développés (c'est-à-dire, exostose), des frontopariétaux solidement fusionnés le long de leur ligne médiane et étendus postéro-latéralement formant un large processus squamosal, des squamosals étendus antéro-postérieurement formant une lamella alaris en forme de plaque, et un maxillaire s'articulant postérieurement avec le quadratojugal pour former une «joue» osseuse solide. La première analyse cladistique incluant *H. szukacsi* confirme son appartenance aux Neobatrachia, mais le place parmi les hyloïdes plutôt que parmi les ranoïdes comme proposé à l'origine. Des indications sur les hyloïdes du continent africain et de Madagascar au cours du Crétacé supérieur, suggèrent que l'ancêtre de *H. szukacsi* a pu se disperser depuis l'Afrique, à travers la proto-Méditerranée et en Europe, avant le Santonien.

MOTS CLÉS
Plaque apulienne , Gondwana, Neobatrachia, Hyloïdes, paléogéographie.

INTRODUCTION

With about 7130 currently recognized extant species and having a nearly cosmopolitan distribution, anurans (frogs and toads) are the most speciose and widespread clade of living amphibians (e.g., Bossuyt & Roelants 2009; Blackburn & Wake 2011; Pyron & Wiens 2011; AmphibiaWeb 2019; Frost 2019). Over 96% of extant anuran species and over 80% of extant anuran families belong to the clade Neobatrachia (e.g., AmphibiaWeb 2019; Frost 2019). Molecular studies generally date the origin and initial diversification of neobatrachians to the Late Triassic-Early Jurassic, prior to the initial break up of Pangea, and then followed in the Late Jurassic-Early Cretaceous, as Pangea began breaking up, by the split between the two major neobatrachian subclades (both sensu Frost *et al.* 2006), Hyloides and Ranoides (e.g., Feller & Hedges 1998; San Mauro *et al.* 2005; Roelants *et al.* 2007; Wiens 2007; Bossuyt & Roelants 2009; Irisarri *et al.* 2012; Zhang *et al.* 2013; Marjanović & Laurin 2014; Pyron 2014; Hedges *et al.* 2015; Frazão *et al.* 2015; Feng *et al.* 2017).

The Mesozoic record for neobatrachians (see reviews by Sanchiz 1998; Roček 2000) is largely limited to former Gondwanan landmasses: in South America from the Aptian-Albian, Turonian-Santonian, and Campanian-Maastrichtian of Brazil and the Campanian-Maastrichtian of Argentina (e.g., Báez 1987; Carvalho *et al.* 2003; Báez *et al.* 2009, 2012; Agnolin 2012; Nicoli *et al.* 2016; Báez & Gómez 2018); in continental Africa from the Cenomanian of Sudan and the Coniacan-Santonian of Niger and, possibly, the Cenomanian of Morocco (Báez & Werner 1996; Báez & Rage 2004; Agnolin 2012); and in the Maastrichtian of both India (e.g., Noble 1930; Špinar & Hodrova 1985; Prasad & Rage 1995, 2004) and Madagascar (Evans *et al.* 2008, 2014).

The first report of a putative neobatrachian of Mesozoic age in Laurasia came in 2010, when *Hungarobatrachus szukacsi* Szentesi & Venczel, 2010 was described on the basis of isolated, distinctive ilia and generalized tibio-fibulae from the Santonian-age Iharkút locality, in northwestern Hungary. Szentesi & Venczel (2010, 2012a) proposed that *Hungarobatrachus* Szentesi & Venczel, 2010 was a neobatrachian based on its ilium having an extremely high dorsal crest and slender ilioischiadic junction. Those authors further suggested that *Hungarobatrachus* might be ranoid or ranoid-like anuran based on its ilium bearing a posterolaterally positioned and laterally projecting, flange-like dorsal protuberance reminiscent of those in Sub-Saharan pyxicephalids, such as the burrowing sand frog *Tomopterna* Duméril & Bibron, 1841. The neobatrachian affinities of *Hungarobatrachus* subsequently have been accepted by several workers (Báez *et al.* 2012; Marjanović & Laurin 2014), with the latter authors also accepting it as a ranoid. By contrast, Roček (2013) regarded *Hungarobatrachus* as an incertae sedis anuran.

TABLE 1. — Inventory of 31 bones known for *Hungarobatrachus szukacsi* Szentesi & Venczel, 2010. Most are incomplete and all are from the SZÁL-6 site at the Iharkút vertebrate locality, Bakony Mountains, northwestern Hungary, in the Upper Cretaceous (Santonian) Csehbánya Formation.

Previously Reported Material
Ilia (n = 7):
MTM V 2008.16.1 [holotype] — Szentesi & Venczel (2010: figs 2A-E, 4A; 2012a: figs 3A-E, 5A); Venczel & Szentesi (2012: fig. 4A, B); this study: Fig. 2E, F.
MTM V 2008.12.1 — Szentesi & Venczel (2010, 2012a); this study.
MTM V 2008.13.1 — Szentesi & Venczel (2010, 2012a); this study.
MTM V 2008.14.1 — Szentesi & Venczel (2010: fig. 3D, E; 2012a: fig. 4D, E); this study.
MTM V 2008.15.1 — Szentesi & Venczel (2010: fig. 3A-C; 2012a: fig. 4A-C); this study.
MTM V 2008.17.1 — Szentesi & Venczel (2010, 2012a); this study.
MTM V 2008.18.1 — Szentesi & Venczel (2010, 2012a); this study.
Tibio-fibulae (n = 5):
MTM V 2008.19.1 — Szentesi & Venczel (2010, 2012a); this study.
MTM V 2008.21.1 — Szentesi & Venczel (2010, 2012a); this study.
MTM V 2008.32.1 — Szentesi & Venczel (2010: fig. 3F, G; 2012a: fig. 4F, G); this study.
PAL 2008.31.1 — Szentesi & Venczel (2010, 2012a: reported in both publications using invalid number MTM V 2008.33.1, according to Dulai *et al.* 2018: 36); this study.
PAL 2008.32.1 — Szentesi & Venczel (2010, 2012a: reported in both publications using invalid number MTM V 2008.34.1, according to Dulai *et al.* 2018: 36); this study.
Newly Reported Material (this study)
Ilia (n = 2):
MTM VER 2015.145.1 — Fig. 2A-D
MTM VER 2015.145.2 — unfigured
Azygous frontoparietal (n = 1):
MTM VER 2016.2546 — Figs 3A-H; 7
Squamosals (n = 6):
MTM VER 2016.695 — Fig. 4G; 7
MTM VER 2016.697.1 — Fig. 4C, D
MTM VER 2016.701.1 — Fig. 4A, B
MTM VER 2016.701.2 — Fig. 4E, F
MTM VER 2016.702 — Fig. 4H, I
MTM VER 2016.3575 — Fig. 4J-L
Maxillae (n = 8):
MTM VER 2010.290.1 — unfigured
MTM VER 2015.141.1 — unfigured
MTM VER 2015.141.2 — Fig. 5H-J
MTM VER 2015.141.3 — Fig. 5K-M
MTM VER 2016.690 — Fig. 5A-C; 7
MTM VER 2016.699 — unfigured
MTM VER 2016.700.1 — Fig. 5G
MTM VER 2016.700.2 — Fig. 5D-F
Angulosplenials (n = 2)
MTM VER 2015.153 — Fig. 6A-C
MTM VER 2016.1948 — Fig. 6D-F

Ongoing collecting efforts at the Iharkút fossil locality have yielded additional ilia and the first skull remains (incomplete frontoparietals, squamosals, maxillae, and angulosplenials) referable to *Hungarobatrachus szukacsi*. Based on all 31 bones currently available for *Hungarobatrachus*, here we: 1) provide an emended diagnosis for *Hungarobatrachus*; 2) describe the newly referred specimens; 3) present a cladistic analysis that tests the proposed neobatrachian and ranoid affinities of *Hungarobatrachus*; and 4) discuss the paleobiogeographic implications of our cladistic analysis.

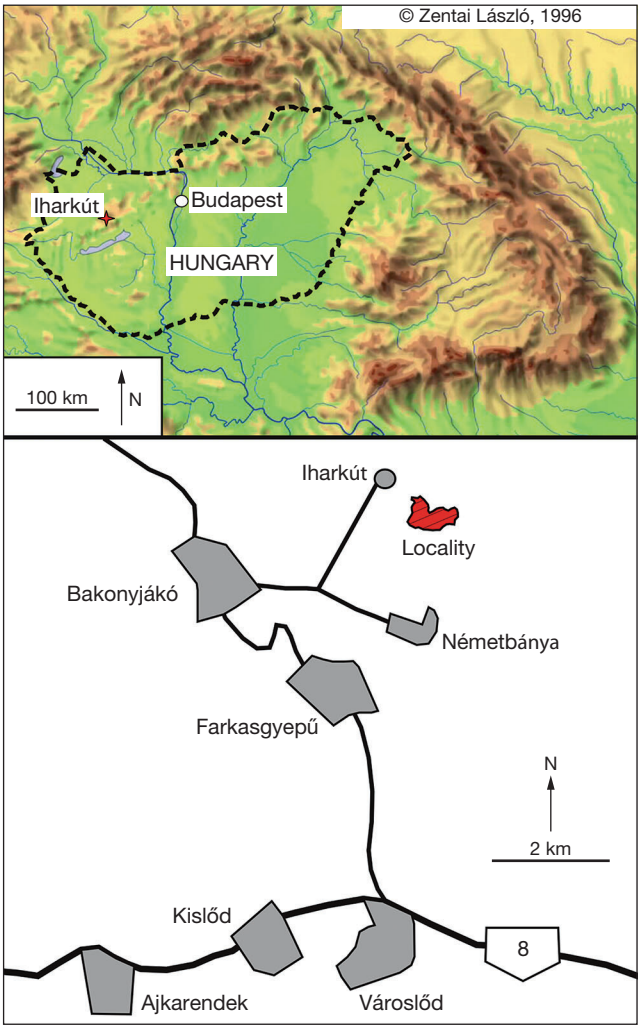

FIG. 1. — Location of the Santonian fossil vertebrate locality of Iharkút, Hungary: **A**, regional map showing approximate location (red star) in the Bakony Mountains of northwestern Hungary; **B**, local map showing location of the open-pit bauxite mine (colored in red) containing the locality, between the villages of Iharkút and Németbánya.

LOCALITY AND GEOLOGICAL SETTING

The Iharkút vertebrate locality lies within an open-pit bauxite mine (Fig. 1), situated between the villages of Iharkút and Németbánya in the Bakony Mountains, northwestern Hungary (e.g., Ősi & Mindszenty 2009; Ősi *et al.* 2012), in an area that during the Mesozoic was positioned on the northern part of the Apulian microplate (Csontos & Vörös 2004). Vertebrate fossils documenting a mix of terrestrial and freshwater taxa (e.g., see Botfalvai *et al.* 2016) are found throughout exposures of the Csehbánya Formation, which is a sedimentary unit deposited in fluvial and floodplain settings during the Santonian (Ősi & Mindszenty 2009; Ősi *et al.* 2012). In the quarry, the most productive sequence (SZÁL-6 site) within exposures of the Csehbánya Formation is a greyish, coarse basal breccia covered with sandstone and brownish siltstone that has produced 99 percent of the identifiable vertebrate fossils (Szabó *et al.* 2016), including all of the *Hungarobatrachus szukacsi* specimens reported here in our paper. Fragmentary

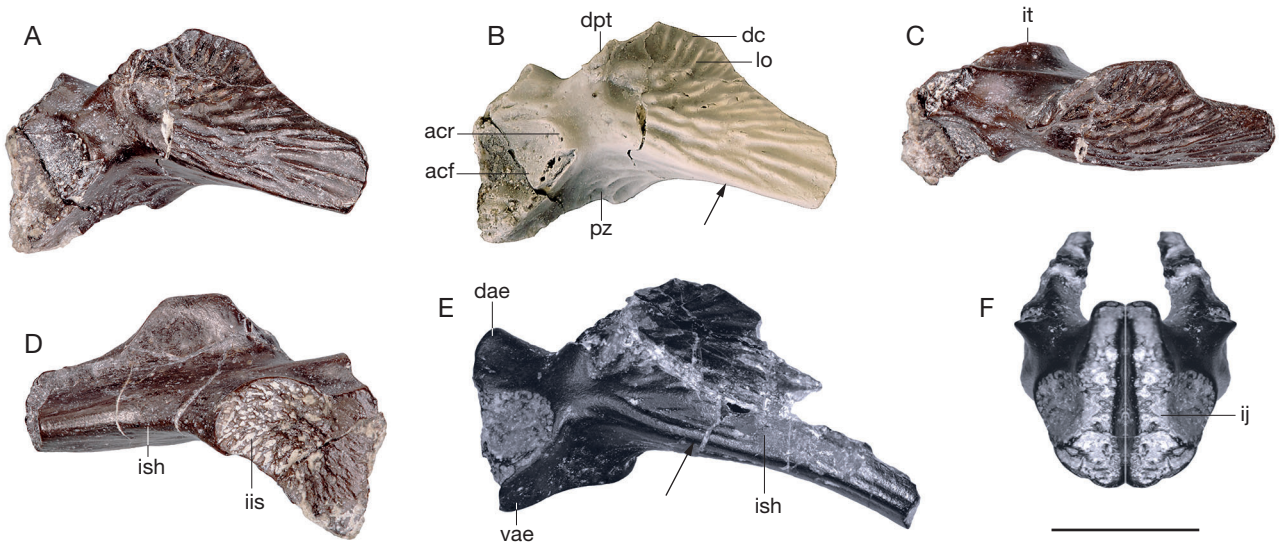

FIG. 2. — Incomplete ilia of *Hungarobatrachus szukacsi* Szentesi & Venczel, 2010 from the Santonian of Iharkút, Hungary: **A**-**D**, MTM VER 2015.145.1, newly referred, right ilium in lateral (**A**, **B**), dorsal (**C**), and medial (**D**) views; **E**, MTM V 2008.16.1, holotype right ilium in lateral view; **F**, Reconstruction of acetabular region in *Hungarobatrachus szukacsi* in posterior view (right ilium is holotype, left ilium is mirror image of holotype). All images are photographs. Specimen in **B** dusted with ammonium chloride to enhance surface details; remaining images are of undusted specimens. Arrows (**B**, **E**) indicate calamita ridge-like rim demarcating lower boundary of ornamented area. Abbreviations: **acf**, acetabular fossa; **acr**, acetabular rim; **dae**, dorsal acetabular expansion; **dc**, dorsal crest; **dpt**, dorsal protuberance; **iis**, interiliac scar; **ij**, ilioischiatic juncture; **ish**, ilial shaft; **it**, interiliac tubercle; **lo**, lateral ornament; **pz**, preacetabular zone; **vae**, ventral acetabular expansion. All images at same magnification. Scale bar: 5 mm.

anuran bones also have been recovered from three other sites (SZÁL-7, -8, and -10) at Iharkút, but those fossils are too fragmentary to be identified beyond Anura indet. Fossils of *Hungarobatrachus* co-occur at Iharkút with those of an alytid frog (Szentesi & Venczel 2012b) and indeterminate albanerpetontids (Szentesi *et al.* 2013).

MATERIAL AND METHODS

All 31 specimens available for *Hungarobatrachus szukacsi* are isolated and incomplete bones from SZÁL-6 site at Iharkút (Table 1). Larger fossils (frontoparietals, ilia, and the most nearly complete maxilla) were collected by hand quarrying, whereas smaller fossils were recovered by screen washing matrix through a series of screens with mesh sizes of 2.00, 1.00, and 0.32 mm. Where safe to do so, adhering matrix was carefully removed with needles and brushes. All *Hungarobatrachus* specimens are curated in the Paleontology collections of the Hungarian Natural History Museum, Budapest. Specimen catalogue numbers in that collection variably bear the prefixes "MTM V", "MTM VER", or "PAL" and, following the format used by Dulai *et al.* (2018), all numbers end with a period. Body size estimates for *Hungarobatrachus* rely on direct comparisons with homologous bones from extant anuran skeletons of known absolute sizes and on the regression formula provided by Esteban *et al.* (1995). Osteological terms generally follow Bolkay (1919) and Roček (1981, 1994) for skull bones and, for ease of comparison with the type description for *H. szukacsi*, generally follow Szentesi & Venczel (2010) for ilia. Digital photographs were taken at the Hungarian Natural History Museum, Budapest, and the Țării Crișurilor Museum, Oradea, Romania, using a Canon EOS digital camera equipped with a 60 mm f/2.8 macro lens and extension tube. Scanning-electron micrographs were taken with a Hitachi S-2600N field emission scanning electron microscope at the Department of Botany, Hungarian Natural History Museum.

SYSTEMATIC PALAEONTOLOGY

Order ANURA Fischer, 1813
Suborder NEOBATRACHIA Reig, 1958
?HYLOIDES
Frost, Grant, Faivovich, Bain, Haas, Haddad, de Sá, Channing, Wilkinson, Donnellan, Raxworthy, Campbell, Blotto, Moler, Drewes, Nussbaum, Lynch, Green & Wheeler, 2006
Genus *Hungarobatrachus* Szentesi & Venczel, 2010

Hungarobatrachus szukacsi Szentesi & Venczel, 2010
(Figs 2-7)

MATERIAL EXAMINED. — 31 isolated and mostly incomplete bones (see Table 1).

DISTRIBUTION. — Known exclusively from the SZÁL-6 site at the Iharkút vertebrate locality, Bakony Mountains, northwestern Hungary, in the Upper Cretaceous (Santonian) Csehbánya Formation.

EMENDED DIAGNOSIS (modified and expanded from Szentesi & Venczel 2010; Roček 2013). — Body size moderate (estimated 50-80 mm snout-vent length). Skull moderately hyperossified. Exostosis on external surfaces of frontoparietals, squamosals, and maxilla generally consists of pit-and-ridge ornament, with some

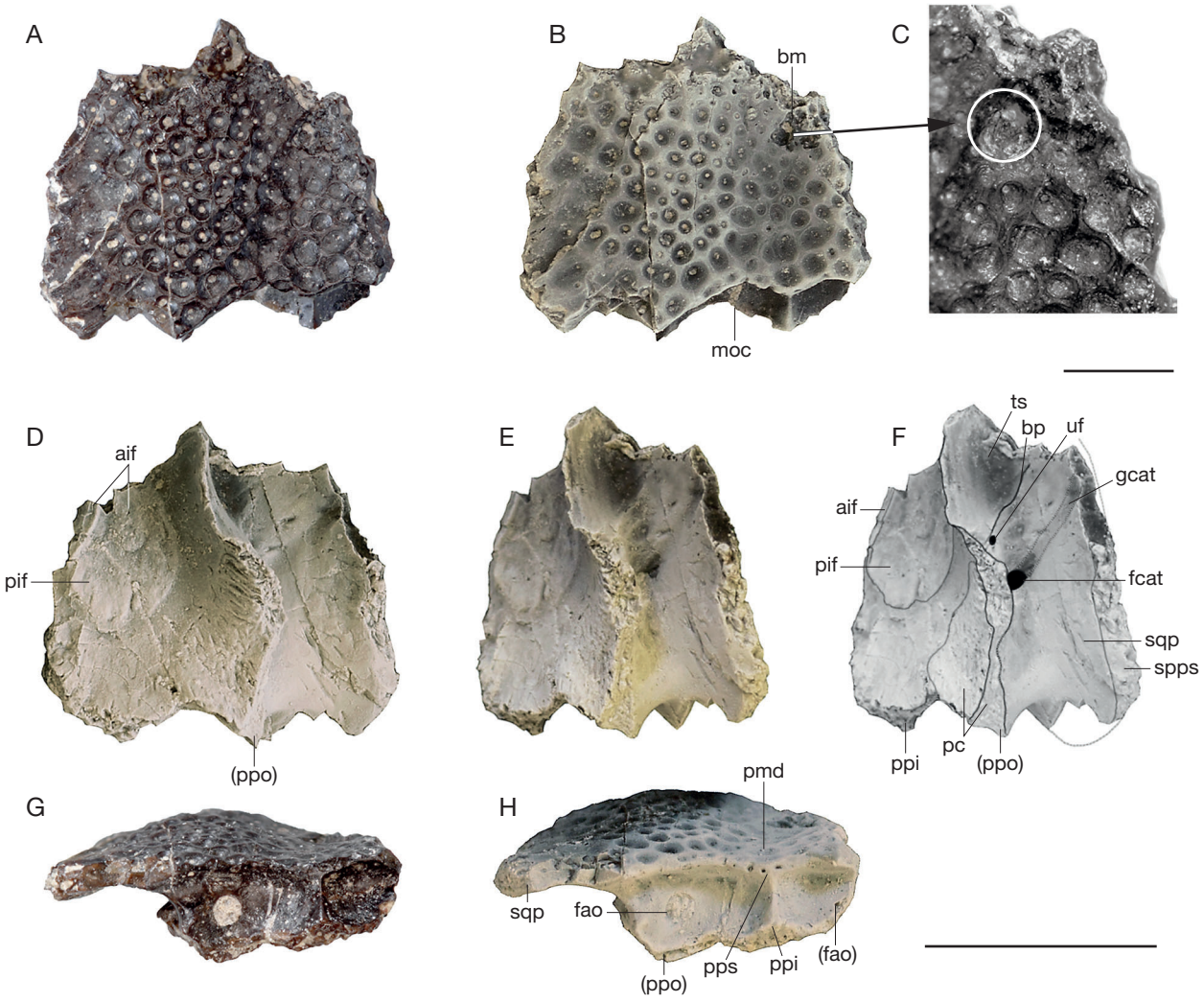

FIG. 3. — Newly referred, incomplete and fused frontoparietals of *Hungarobatrachus szukacsi* Szentesi & Venczel, 2010 from the Santonian of Iharkút, Hungary: **A**-**H**, MTM VER 2016.2546, posteromedian and left posterolateral portions of a fused pair of frontoparietals, entire specimen in dorsal (**A**, **B**) views, enlargement of dorsal surface with putative bite mark circled (**C**), entire specimen in ventral view (**D**), entire specimen in oblique ventral and slightly left lateral view as both a photograph (**E**) and interpretive image (**F**), and entire specimen in posterior view (**G**, **H**). Photographs in **B**, **D**, **E**, and **H** dusted with ammonium chloride to enhance surface details; remaining images are of undusted specimens. Abbreviations: **aif**, anterior incrassiato frontoparietalis; **bm**, putative bite mark; **bp**, bony pillar extending dorsally along lateral surface of pars contacta onto underside of squamosal process; **gcat**, groove for canalis arteria temporalis; **fao**, intact left foramen arteriae occipitalis; **(fao)**, preserved medial rim of right foramen arteriae occipitalis; **fcat**, foramen canalis arteria temporalis; **moc**, intact medial portion of margo occipitalis; **pc**, pars contacta; **pif**, posterior incrassatio frontoparietalis; **pmd**, posteromedian depression; **ppi**, processus posterior inferior; **(ppo)**, broken base of processus paraoccipitalis; **pps**, processus posterior superior; **spps**, surface of postorbital parasagittal suture; **sqp**, squamosal process; **ts**, tectum supraorbitale; **uf**, unidentified foramen. Images at different magnifications. Scale bar: A, B, D-H, 5 mm; C, 1 mm.

weakly developed tuberculate ornament on lower portions of larger squamosals and adjacent portion of maxillae. Frontoparietals solidly fused along midline and no development of dorsal crests or ridges, at least posteriorly; posterolateral portion expanded laterally to form a large squamosal process that potentially contacts laterally with squamosal; ventral surface bears two unpaired frontoparietal incrassations, consisting of an evidently elongate anterior incrassation with a bi-lobed posterior margin and a subcircular posterior incrassation; and occipital canal completely enclosed within bone, with its foramen arteria temporalis opening ventrally between squamosal process and pars contacta. Squamosal having enlarged, ventroanteriorly directed processus zygomaticus and smaller, posteriorly directed processus posterodorsalis, both expanded to form broad lamella alaris that is tilted posteriorly, somewhat rhomboid in outline, with anterodorsal margin shallowly concave and fully enclosing posterior portion of orbit and with posteroventral margin more deeply concave; base of processus zygomaticus expanded anteroposteriorly and evidently abutted against complementary processus zygomatico-maxillaris on maxilla; anteroventral end of processus zygomaticus moderately elongate and tapered, with leading edge bearing tiny, knob-like projections. Maxilla moderately elongate, deep, and robust; preorbital region deepest, orbital region indented by moderately elongate and concave margo orbitalis, and postorbital region moderately deep, elongate, and tapered posteriorly; lamina horizontalis deep and lingually narrow, ending posteriorly in an evidently well developed processus pterygoideus; processus posterior lingually bears sutural surface for quadratojugal articulation, indicating maxillary arcade was closed posteriorly forming a bony 'cheek'; and maxilla dentate, bearing numerous small and closely spaced teeth. Angulosplenial having processus coronoideus bearing single low, broadly convex dorsal tubercle. Ilium heavily built; dorsal crest high (about 2.5 times higher than ilial shaft) and sail-like in lateral outline, and mediolaterally thick; lateral surface of dorsal crest and adjacent dorsolateral surface of shaft prominently

ornamented with anteroposteriorly elongate grooves and posteriorly anastomosing ridges, with ornamented surface demarcated ventrally by a convex ridge extending anteroposteriorly along lateral surface of ilial shaft; dorsal protuberance developed as a medially thickened, low, and laterally projecting flange, with undivided and roughened surface; interiliac tubercle greatly enlarged to cover entire medial portion of ilial body including preacetabular region and with its medial surface flattened and variably roughened for strong sutural contact with opposite ilium.

Description of newly referred material

General remarks

The seven ilia and five tibio-fibulae originally reported for *Hungarobatrachus szukacsi* were thoroughly documented in English by Szentesi & Venczel (2010) in the type description and later in Hungarian by the same authors (Szentesi & Venczel 2012a). No additional tibio-fibulae are known, but another two ilia are now available. Our descriptions and remarks below focus on the new ilial specimens and on newly recognized skull bones (incomplete frontoparietals, squamosals, maxillae, and angulosplenials). Most new examples of those elements are depicted in Figs 3-6 and our tentative reconstruction for the skull of *Hungarobatrachus* is presented in Figure 7. On the basis of ilia and tibio-fibulae then available, Szentesi & Venczel (2010) estimated a body size of 50-60 mm for *Hungarobatrachus*. The largest of the newly recognized squamosals and maxillae suggest a higher upper size range, of about 80 mm.

Ilium (Fig. 2)

Consistent with the seven ilia previously reported for *Hungarobatrachus szukacsi* (e.g., Szentesi & Venczel 2010: figs 2, 3A-E, 4A), both of the newly referred ilia preserve much of the ilial body (= acetabular region) and the posterior portion of the ilial shaft. The more nearly complete of the two new ilia, MTM VER 2015.145.1 (Fig. 2A-D), is comparable in size to the holotype ilium (cf., Szentesi & Venczel 2010: fig. 2; this study: Fig. 2E, F), although the former preserves less of its supra- and subacetabular regions and dorsal crest. The other newly referred example, MTM VER 2015.145.2 (not figured), is less intact. Our abbreviated description below focuses on the better preserved and figured specimen, MTM VER 2015.145.1.

The ilium is heavily built and robust. In lateral view, the ilial body is triangular in outline; the acetabular fossa is fully enclosed within the ilial body, shallowly concave in medial depth, sub-circular in outline, and bordered anteroventrally by a low acetabular rim; the dorsal acetabular expansion is moderately tall and lacks a supraacetabular fossa; the ventral acetabular expansion is relatively shallower; and the preacetabular zone is moderately expanded anteroventrally in the form of an asymmetrically convex bulge that is confluent medially with the enlarged interiliac tubercle. In medial view, the interiliac tubercle covers the entire medial face of the ilial body and even expands anteriorly across the preacetabular region to connect with the posteriormost portion of the ilial shaft. The enlarged interiliac tubercle is triangular in dorsal or ventral view, being medially thickest anteriorly and narrowing posteriorly, and its medial face is broad, flattened, and covered by a roughened surface that we call the "interiliac scar" (sensu Gómez & Turazzini 2016). The preacetabular angle (i.e., angle between anterior margin of ventral acetabular expansion and ventral surface of ilial shaft, measured in lateral aspect) is slightly more than 90°. The ilial shaft is cylindrical in cross section and, extending along its dorsolateral surface, bears a prominent dorsal crest. The crest is both tall (about 2.5 times taller than ilial shaft and with dorsal edge of crest lying well above level of dorsal surface of acetabular dorsal expansion) and mediolaterally thickened. The posterior end of the dorsal crest is approximately in line with the anterior portion of the acetabular rim and lies well behind the anterior limit of the anteriorly expanded interiliac tubercle. The dorsal crest projects dorsally and slightly medially; its medial face is flattened and smooth, whereas its lateral face is shallowly convex. Prominent ridge-and-groove ornament is developed across the lateral surfaces of the dorsal crest and the dorsal three-quarters of the underlying ilial shaft. The lowermost boundary of that ornamented area is sharply defined by a narrow, but prominent ridge extending along the ventrolateral surface of the ilial shaft; that ridge is in approximately the same position as the calamita ridge reported in some bufonids (see Gómez & Turazzini 2016: 8), but is not clearly homologous with the latter structure. Along the shaft and onto the lower two-thirds of the dorsal crest, the lateral ornament on MTM VER 2015.145.1 consists of anteroposteriorly elongate grooves and posteriorly anastomosing ridges, whereas across the upper one-third of the crest the ridges are shorter and oriented more vertically. Along its posterior edge, the dorsal crest bears a dorsal protuberance in the form of a low and moderately thickened flange that projects laterodorsally and has a slightly roughened surface.

In their preserved features, both newly referred ilia are virtually identical to those previously reported for *Hungarobatrachus szukacsi*, especially in exhibiting the seemingly unique combination of an enlarged interiliac tubercle and a prominent dorsal crest ornamented laterally with pronounced ridges and grooves. Several features known for the originally described ilia are not preserved in either of the new specimens. These include: 1) orientation and posterior extent of the dorsal acetabular expansion, which in the holotype is oriented dorsoposteriorly at a shallow angle and was inferred not to have borne a posteriorly tapered ischiadic process that projected beyond the posterior limit of the acetabular fossa (Fig. 2E); 2) medial outline of the interiliac tubercle, which in the holotype resembles a bell tilted onto its side (Szentesi & Venczel 2010: fig. 2C); 3) form of ilioischiadic juncture, which in the holotype is mediolaterally thin and its posterior face is smooth and shallowly concave from side-to-side (Fig. 2F); and 4) lateral outline of the dorsal edge of the dorsal crest, which on two of the previously referred ilia is seen to be broadly arcuate and dipping anteriorly (Szentesi & Venczel 2010: figs 3A, D). The newly referred and figured ilium (MTM VER 2015.145.1) corroborates earlier reports that the interiliac scar, which is broadly developed

across the medial surface of the interiliac tubercle, may be either roughened (e.g., MTM VER 2015.145.1: Fig. 2D; previously referred MTM V 2008.15.1: Szentesi & Venczel 2010: fig. 3C) or nearly smooth (e.g., holotype MTM V 2008.16.1: Szentesi & Venczel 2010: fig. 2C). Those differences in surface texture imply corresponding differences in the relative strength of the interiliac joint. Intriguingly, those textural differences do not appear to be size-related. Finally, MTM VER 2015.145.1 exhibits a slightly different pattern of lateral ornament on the dorsal crest, with ridges across the upper one-third of its crest being short and extending more vertically, rather than being oriented more horizontally as in the holotype (cf., Fig. 2A, B versus Fig. 2E). We do not regard that minor variant in lateral ornament as being taxonomically significant.

Frontoparietal (Fig. 3)

The only available specimen, MTM VER 2016.2546, represents the posteromedian and adjacent left posterolateral portion of an azygous (i.e., fused) pair of frontoparietals. The specimen is a small (maximum width = 7.5 mm and maximum anteroposterior length = 6.9 mm) and relatively flat piece of bone, with a somewhat pentagonal dorsal or ventral outline (Fig. 3A, B, D). Most of the margins are broken surfaces; the only intact margins are an anteroposteriorly short portion along the left posterolateral edge (Fig. 3D-F) and a moderately broad portion across the middle of the occipital (posterior) surface (Fig. 3G, H). Due to breakage, the overall size, proportions, and shape of the azygous frontoparietals are largely unknown. Nevertheless, enough of the posterolateral portion is preserved on the left side to show that region is moderately expanded both laterally and anteroposteriorly (see below). Additionally, the specimen is traversed by several major cracks and, along its sagittal midline, is indented by a small, sub-circular divot (Fig. 3B, C) that may represent a bite or puncture mark.

Although MTM VER 2016.2546 is incomplete and broken asymmetrically, its sagittal midline (Fig. 3G, H) can be recognized using two sets of landmarks along the occipital surface: 1) a dorsally placed processus posterior superior and a ventrally placed processus posterior inferior that both project a short distance posteriorly from the posterior midline; and 2) an equal distance from, and to either side of, the posterior midline, the occipital face of the specimen is perforated by an intact (left) and incomplete (right) opening for the foramen arteriae occipitalis. The dorsal and ventral surfaces of MTM VER 2016.2546 lack a suture or a line of fusion demarcating the sagittal midline. Instead, the bone is solid and continuous throughout that region. This indicates that the left and right frontoparietals were solidly fused, at least along the posterior portions of their medial edges. Based on comparisons with other anurans having solidly fused frontoparietals, we predict that the left and right frontoparietals were solidly fused together along their entire lengths in *Hungarobatrachus*.

The facies dorsalis or roofing portion of MTM VER 2016.2546 is moderately thick, becoming slightly thicker posteriorly, and is essentially horizontal. In anterior (not shown) and posterior (Fig. 3G, H) views, the median portion of the facies dorsalis is shallowly depressed along the sagittal midline, similar to the extant calyptocephalellid *Calyptocephalella gayi* (Lynch 1971: fig. 20B, depicted as *Caudiverbera caudiverbera*) and the Eocene ranoid *Thaumastosaurus* De Stefano, 1903 (Roček & Lamaud 1995: fig. 2B; Rage & Roček 2007: fig. 1D; Laloy *et al.* 2013: fig. 3D). On the left side, enough of the posterolateral portion is preserved to show that the processus lateralis superior is expanded both laterally and anteroposteriorly to form a broad flange that we call the "squamosal process". This process projects laterally in a shallowly convex arc (Fig. 3G) and, in life, would have overhung the prootic region and at least partially enclosed the posterior margin of the orbital opening (Fig. 7). Best seen in oblique ventral and left lateral view (Fig. 3E, F), the posterior portion of the lateral surface of the squamosal process is intact and roughened. We provisionally interpret this anteroposteriorly roughened surface as a sutural surface for contact laterally with the squamosal. We are forced to qualify that statement, because none of the six available squamosals (see next section) preserves evidence of a complementary contact surface along their dorsal margin. As Lynch (1971: 46-47) noted, many anuran genera have frontoparietals with a posterolaterally expanded portion that approaches, but fails to directly contact with the dorsal rim of the squamosals—that potentially could be the pattern in *Hungarobatrachus*. Regardless of whether the frontoparietal laterally contacted the squamosal, it is evident that the posterolateral portion of the frontoparietal was broader relative to the more anterior portion of the bone. In dorsal or ventral outline, the intact frontoparietals would have resembled an inverted 'T' (Fig. 7).

The entire dorsal surface of MTM VER 2016.2546 exhibits modest exostosis, in the form of pit-and-ridge style ornament (Fig. 3A-C). The pits are of varying diameters and outlines, ranging from small to moderate and oval, sub-circular, or polygonal, but are consistently shallowly concave and their floors are perforated by one or several tiny holes. The pits are bordered by low, narrow ridges that coalesce to form a loosely reticulate arrangement. Although variation is evident in the size and outlines of the pits and ridge, there is no obvious change in ornament across the preserved posterior portion of the frontoparietals. A similar pit-and-ridge ornament occurs on the external surfaces of the squamosals and maxillae. Aside from its dorsal ornamentation and the previously mentioned, possible bite mark, the dorsal surface of MTM VER 2016.2546 lacks other prominent surface features such as crests or ridges. There is no dorsal exposure of the canal for the arteria occipitalis (see below), which indicates that at least along its posterior portion that canal is fully enclosed within the frontoparietal.

Returning to its ventral surface, MTM VER 2016.2546 exhibits several notable features (Fig. 3D-F). Midway across the specimen, the posterior portion of the pars contacta is preserved as a moderately deep and ventrally projecting flange that traces a sinuous anteroposterior path. Along its preserved

anterior portion, the pars contacta is anteroposteriorly straight in ventral view. In this region, the pars contacta laterally bears a weak bony pillar that extends dorsally and then curves laterally onto the underside of the facies dorsalis to demarcate the shallowly concave, posteromedial wall of the orbit. Lateral to the preserved anterior portion of the pars contacta, enough of the laterally expanded portion of the facies dorsalis remains in front of the bony pillar and squamosal process to show that the tectum supraorbitale (= alae supraorbitale) overhung the orbital region, although how far it projected laterally is unknown because the margo orbitalis is not intact. Midway along its length, the pars contacta thickens and flares laterally and, in this region, its ventromedial and ventral surfaces are roughened for sutural contact with the underlying (and not preserved) endocranium. Posteriorly the pars contacta grades into the ventral surface of the pars facialis, but here the bone is broken away where the processus paraoccipitalis would have projected posteriorly. Best seen in oblique ventral and left lateral view (Fig. 3E, F), a moderately large foramen opens midway along the lateral base of the pars contacta. We interpret this opening as the foramen arteria temporalis, for exit of one of the branches of the arteria occipitalis. Extending from that foramen is a shallow groove for the canalis arteria temporalis, which traces the anterolateral path of the arteria temporalis between the ventral surface of the squamosal process and the underlying temporal musculature (Roček 1981). Anterior to the foramen arteria temporalis, a smaller foramen of uncertain identity also opens laterally in the base of the pars contacta. Medial to the pars contacta, the ventral midline of the fused frontoparietals bears slightly thickened bony imprints or patches that represent the incompletely preserved incrassatio frontoparietalis (Fig. 3D). Anteriorly is the posterior portion of what appears to be an unpaired anterior incrassatio frontoparietalis (= facies cerebralis anterior) having a bilobed posterior margin with the indentation at the midline, whereas more posteriorly is a broader, sub-circular, and unpaired posterior incrassatio frontoparietalis (= facies cerebralis posterioris).

Squamosal (Fig. 4)

Six incomplete squamosals are available. Specimens range in size, with the largest (MTM VER 2016.695: Fig. 4G) being about 20 mm in its maximum preserved dimension and, when complete, would have been about twice as large as the smallest example (MTM VER 2016.701.2: Fig. 4E, F). Although no specimen is intact, collectively these demonstrate that the squamosal retained the tri-radiate structure typical for anurans. For *Hungarobatrachus*, its tri-radiate squamosal consists of a prominent and anteroventrally projecting processus zygomaticus (= anterior or zygomatic ramus), a less prominent and posteriorly directed processus posterodorsalis (= posterior or otic process/ramus), and a processus posterolateralis (= squamosal shaft or ventral ramus) of uncertain form and, presumably, directed ventroposteriorly.

The main portion of the squamosal in *Hungarobatrachus* is formed by the processus zygomaticus, portions of which are preserved in all six specimens (Fig. 4), and by the smaller processus posterodorsalis, portions of which are preserved in the first five of the illustrated specimens (Fig. 4A-I). Both processes are conjoined and expanded into a broad plate, the lamella alaris. In lateral and medial views (Fig. 4), the lamella alaris is tilted posteriorly, with its long axis extending ventroanteriorly-dorsoposteriorly, and is somewhat rhomboid in outline, with its anterodorsal margin (margo orbitalis) shallowly concave and its posteroventral margin deeply concave. In anterior and posterior views (not shown), the lamella alaris is moderately thick and bent, with about its lower two-thirds oriented essentially vertically and its upper one-third tilted mediodorsally. The processus posterodorsalis portion of the lamella alaris is moderately deep and projects a short distance posteriorly. The available size range of specimens indicates that the processus posterodorsalis becomes deeper and its posterior end becomes more broadly rounded with increased size (cf., Fig 4E vs. G). The lower margin of the processus posterodorsalis and the posteroventral margin of the processus zygomaticus together form a concave margin that becomes relatively deeper with increased size and, in life, may have bordered the anterior margin of the cartilaginous tympanic annulus (Fig. 7). The dorsal margin of the lamella alaris is formed posteriorly by the processus posterodorsalis and anteriorly by the processus zygomaticus; it is broadly convex in lateral outline and, as noted in the frontoparietal account above, its dorsal and dorsomedial surfaces lack clear evidence of sutural contact with the frontoparietal. The remaining margins of the lamella alaris are formed exclusively by the processus zygomaticus. The margo orbitalis is long, shallowly concave, and faces anterodorsally to completely enclose the posterior and posteroventral margins of the orbital opening (Fig. 7). The ventral edge of the processus zygomaticus is nearly straight or shallowly concave in lateral or dorsal outline and lateromedially thin. The relatively smooth ventral surface of the processus zygomaticus suggests it abutted against the complementary processus zygomatico-maxillaris on the maxilla (see next account). Preserved for two squamosal specimens (MTM VER 2016.695 and 2016.3575: Fig. 4G and Fig. 4J-L, respectively), the anteroventral end of the processus zygomaticus is notable for being moderately elongate and tapered anteriorly, and, in MTM VER 2016.3575 (Fig. 4J-L), its leading edge bears tiny, knob-like projections. This anterior projection is reminiscent of some anurans, such as *Thaumastosaurus* (Rage & Roček 2007: fig. 1A, C; Laloy *et al.* 2013: fig. 3A, C) in which the anteroventral end of the squamosal extends anteriorly along the dorsal edge of the maxilla and contacts the posteriorly expanded nasal, thereby excluding the maxilla from the orbital margin. Although we lack any articulated specimens that unequivocally demonstrate the pattern of squamosal-maxilla contact in *Hungarobatrachus*, the form of the anteroventral end of the isolated squamosals is potentially suggestive of that contact pattern (Fig. 7). If squamosal-nasal contact existed, that may have been strengthened by the tiny, knob-like projections on the leading end of the anterior projection of the squamosal.

The external surface of the lamella alaris is variably ornamented. The available size series indicates that with increased

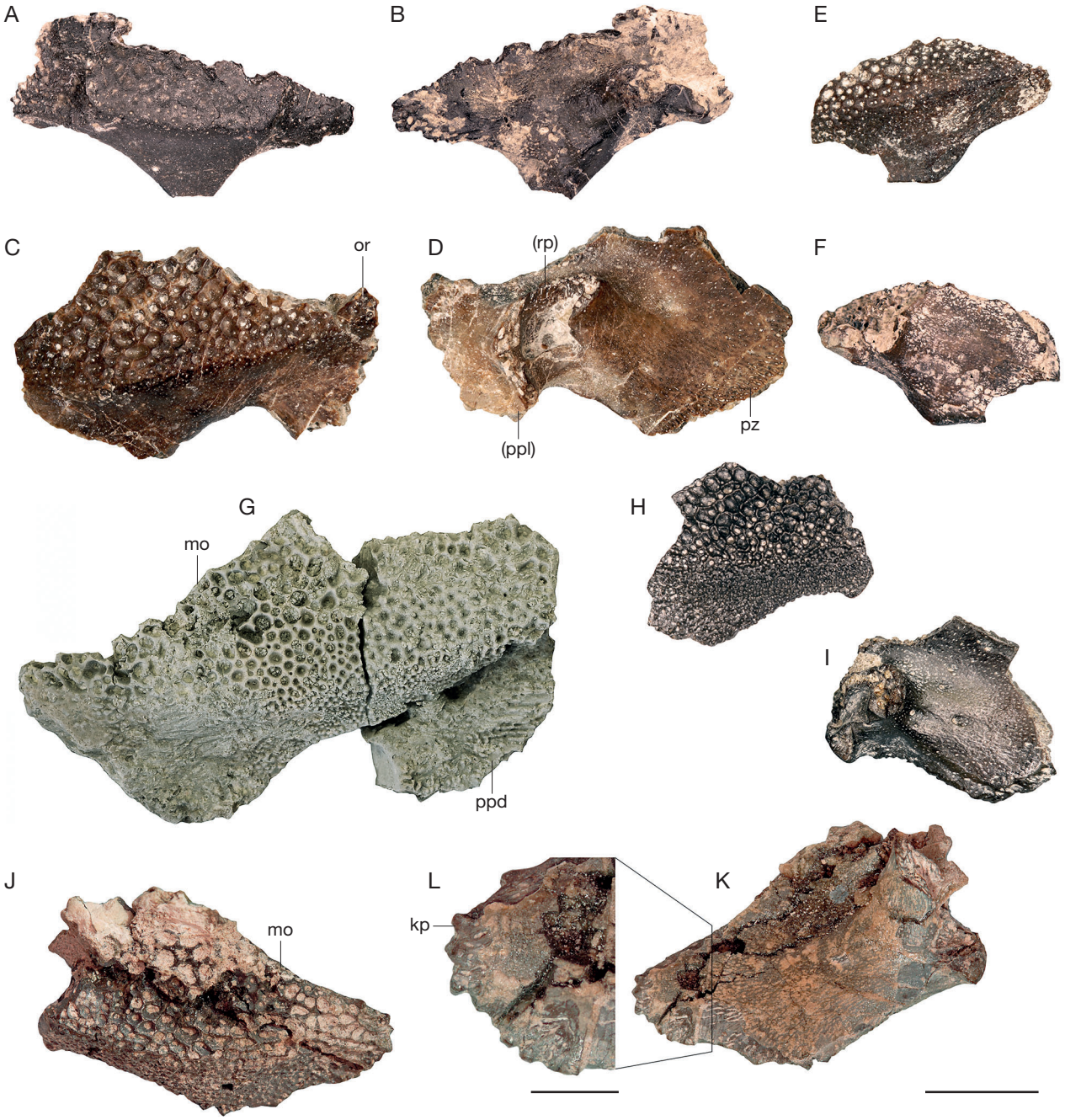

FIG. 4. — Newly referred, incomplete squamosals of *Hungarobatrachus szukacsi* Szentesi & Venczel, 2010 from the Santonian of Iharkút, Hungary: **A**, **B**, MTM VER 2016.701.1, right squamosal in lateral (**A**) and medial (**B**) views; **C**, **D**, MTM VER 2016.697.1, left squamosal in lateral (**C**) and medial (**D**) views; **E**, **F**, MTM VER 2016.701.2, left squamosal in lateral (**E**) and medial (**F**) views; **G**, MTM VER 2016.695, left squamosal in lateral view; **H**, **I**, MTM VER 2016.702, left squamosal in lateral (**H**) and medial (**I**) views; **J**-**L**, MTM VER 2016.3575, right squamosal, entire specimen in lateral (**J**) and medial (**K**) views and detail (**L**) of anterior margin of processus zygomaticus in medial view. All images are photographs. Specimen in **G** dusted with ammonium chloride to enhance surface details; all other images are of undusted specimens Abbreviations: **kp**, tiny knob-like projections on anteroventral end of processus zygomaticus; **mo**, margo orbitalis; **ppd**, processus posterodorsalis; **(ppl)**, broken base of processus posterolateralis; **pz**, processus zygomaticus; **(rp)**, broken base of ramus paroticus. Scale bars: A-K, 5 mm; L, 2 mm.

squamosal size, ornament becomes both more pronounced and its coverage increases. In smaller specimens about the posterior one-third of the lamella alaris is unornamented and smooth, whereas in larger specimens the ornamented area covers the entire lamella alaris (cf., Fig. 4A, C vs Fig. 4G, J). Ornament patterns also vary dorsoventrally across the squamosal. The upper, medially tilted portion of the lamella alaris bears pit-and-ridge style ornament similar to that on the frontoparietals. That gives way to a more loosely reticulate and somewhat tuberculate pattern across the middle and onto the ventral portions of the lamella alaris. In medial view, three specimens preserving the dorsal portion retain the broken, cup-shaped base of the medially directed ramus paroticus (Fig. 4D, F, I); those bases are too incomplete to establish

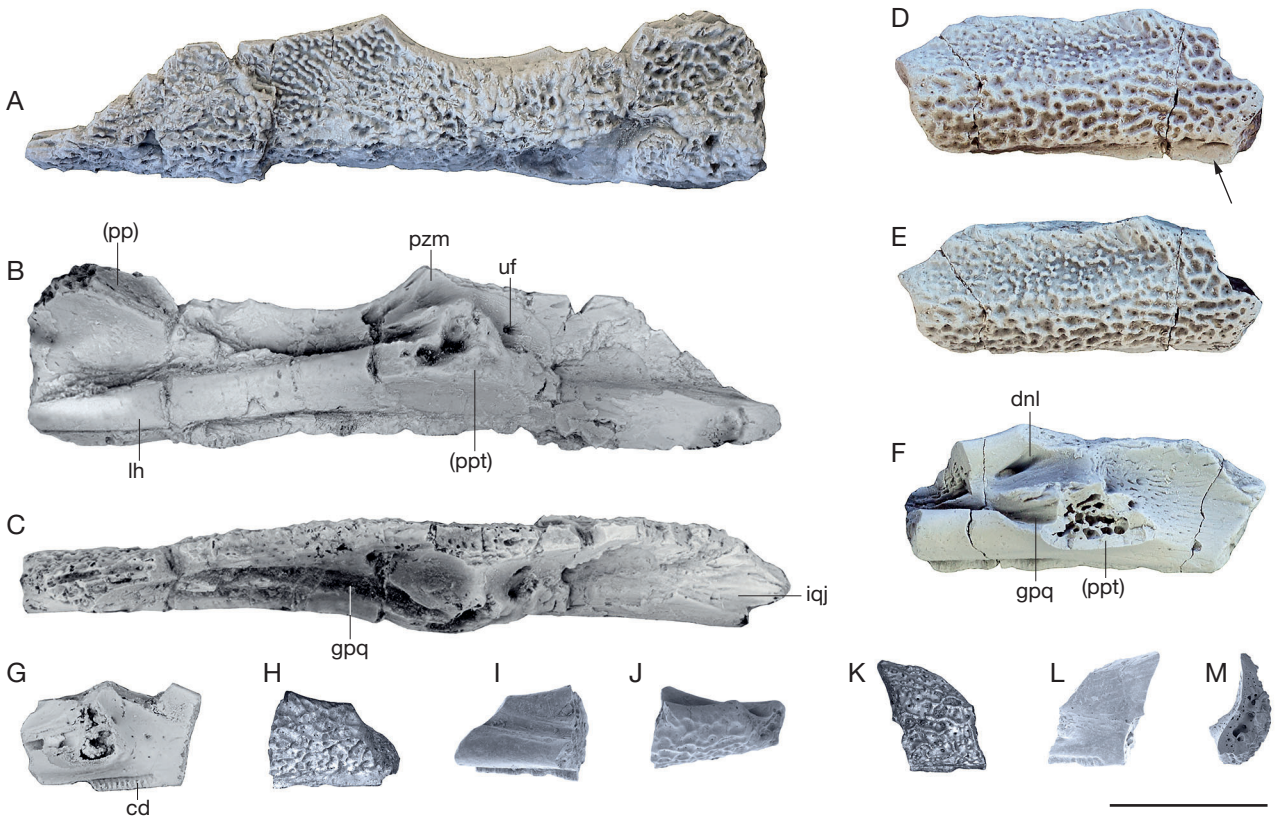

Fig. 5. — Newly referred, incomplete maxillae of *Hungarobatrachus szukacsi* Szentesi & Venczel, 2010 from the Santonian of Iharkút, Hungary: **A**-**C**, MTM VER 2016.690, nearly complete right maxilla in labial (**A**), lingual (**B**), and oblique dorsal and slightly lingual (**C**) views; **D**-**F**, MTM VER 2016.700.2, fragmentary right maxilla preserving region bearing processes pterygoideus (broken) in labial (**D**), oblique labial and slightly dorsal (**E**), and lingual (**F**) views; **G**, MTM VER 2016.700.1, fragmentary right maxilla preserving less of region bearing processus pterygoideus (broken) in lingual view; **H**-**J** MTM VER 2015.141.2, fragmentary right maxilla preserving posterior portion of suborbital region in labial (**H**), lingual (**I**), and dorsal (**J**) views; **K**-**M** MTM VER 2015.141.3, fragmentary right maxilla preserving posterior portion of tooth row in labial (**K**), lingual (**L**), and posterior (**M**) views. Images in **A**-**G** are photographs of specimens dusted with ammonium chloride to enhance surface details; images in **H**-**M** are scanning electron micrographs. Abbreviations: **cd**, crista dentalis; **dnl**, ductus nasolacrimalis; **gpq**, groove for pars palatina palatoquadrati; **iqj**, imprint marking contact area for quadratojugal; **lh**, lamina horizontalis; **(pp)**, broken base of processus palatinus; **(ppt)**, broken base of processus pterygoideus; **pzm**, processus zygomatico-maxillaris; **uf**, unnamed foramen. Arrow (**D**) points to unornamented area along ventrolabial surface of maxilla. All images at same magnification. Scale bar: 5 mm.

the form of the ramus paroticus and its pattern of contact with the complementary crista parotica on the braincase. At least two of those same specimens (Fig. 4D, I) also preserve the broken base of the processus posterolateralis. Considering that the processus posterolateralis is universally present in anurans as a ventroposteriorly projecting strut that invests the palatoquadrate and helps brace the jaws against the braincase (e.g., Trueb 1973, 1993), we assume a similar form and function for *Hungarobatrachus*.

Maxilla (Fig. 5)

Eight maxillae are available. Most are fragmentary, but one (MTM VER 2016.690: Fig. 5A-C) is nearly complete and, except where indicated otherwise, forms the basis for our maxillary description. MTM VER 2016.690 is a right maxilla preserving most of the bone. It is missing its anteriormost end, the anterodorsal portion of its processus frontalis, and much of its processus pterygoideus. Additionally, the ventral edge of the maxilla is damaged along much of the tooth row and no teeth are preserved. Finally, several vertical cracks extending through the maxilla have caused minor labiolingual displacement of adjacent portions. As preserved, MTM VER 2016.690 is about 22 mm long and, when complete, the maxilla was probably about 25 mm long. The long axis of the maxilla curves anteriorly in an extremely shallow arc (Fig. 5C). In cross section, the interior of the bone is perforated by small canals and its labial surface is labially convex (Fig. 5M). The maxilla is relatively robust in its construction.

In labial or lingual outline, MTM VER 2016.690 (Fig. 5A, B) is elongate and moderately deep. Although broken anteriorly, it is clear that the preorbital region was the deepest portion of the maxilla. Judging by its preserved portion, the processus frontalis was a moderately deep flange, as is typical for many anurans. By comparison, the postorbital region is slightly lower, much more elongate, and tapers posteriorly. This region consists anteriorly of a processus zygomatico-maxillaris that is deepest anteriorly. Behind its weakly triangular apex, the dorsal edge of the processus zygomatico-maxillaris is shallowly concave and descends at a shallow angle posteriorly to a point about three-fifths of the distance along the postorbital region; at that point, the dorsal edge of the bone descends at a steeper angle and terminates posteriorly in a

FIG. 6. — Newly referred, incomplete angulosplenials of *Hungarobatrachus szukacsi* Szentesi & Venczel, 2010 from the Santonian of Iharkút, Hungary: **A**-**C**, MTM VER 2015.153, left angulosplenial in dorsal (**A**), lingual (**B**), and posterior (**C**) views; **D**-**F**, MTM VER 2016.1948, left angulosplenial in lingual (**D**) and dorsal (**E**, **F**) views. All images are photographs. Specimen in **F** dusted with ammonium chloride to enhance surface details; remaining images are of undusted specimens. Abbreviations: **(ec)**, broken posterior part of extremitas cultellata; **es**, extremitas spatulata; **pc**, processus coronoideus; **spcM**, sulcus pro cartilage Meckeli. Arrows point to coronoid tubercle. All images at same magnification. Scale bar: 2 mm.

low and blunt processus posterior. Separating the pre- and postorbital regions, the orbital region is moderately elongate and its margo orbitalis is shallowly concave.

MTM VER 2016.690 and more fragmentary specimens show that much of the labial surface of maxilla is ornamented, except for a shallow strip along the ventralmost portion corresponding to the crista dentalis (= pars dentalis) (Fig. 5A, D, H, K). The ornament pattern varies across the labial surface of the maxilla. On both MTM VER 2016.690 and 2016.700.2 (Fig. 5A and D, E, respectively), about the upper one-half of the processus zygomatico-maxillaris and adjacent portion of the orbital region are ornamented with small tubercles that may be isolated, but more typically are aligned and joined into short, broken ridges; this resembles the labial ornament on the adjacent, lower portion of the squamosals. The remainder of the labial surface of the maxilla bears irregular pit-and-ridge ornament.

A substantial portion of the lingual surface of the maxilla is preserved on MTM VER 2016.690 (Fig. 5A). Best developed along the suborbital region, the lamina horizontalis (= pars palatinus) is a moderately deep (i.e., accounts for about one-third of the suborbital depth) and lingually narrow ledge, with a shallowly convex labial face and a broad groove along its dorsal surface. Anteriorly, the lamina horizontalis shallows and its anteriormost end is broken away. More posteriorly, the lamina horizontalis deepens and expands lingually as it grades into the broken base of the processus pterygoideus. Although no maxillary specimen preserves more than the broken base of that process (Fig. 5B, F, G), those remnants indicate that the processus pterygoideus would have been relatively well developed (although its shape and lingual extent are uncertain) and, as in most anurans, would have articulated with the pterygoid. In life, the pars palatina palatoquadrati would have fit into the deep dorsal groove that extends anteriorly from the processus pterygoideus onto the dorsal surface of the lamina horizontalis (Fig. 5C, F). Because the anterior and anterodorsal portions of the maxilla are missing, patterns of contact with the premaxilla anteriorly and the nasal anterodorsally cannot be determined (Fig. 7). Along its preserved lingual surface, the processus frontalis bears the anterodorsally directed, broken base of the processus palatinus. The ductus nasolacrimalis is enclosed by bone along the upper part of the suborbital region and opens posteriorly as a foramen above the base of the processus pterygoideus. A second, unidentified foramen opens more posteriorly, behind the base of the processus pterygoideus. As noted in the squamosal description above, the dorsal and dorsoventral surfaces of the processus zygomatico-maxillaris lack obvious sutural surfaces for contacting the squamosal; instead, those two bones probably simply abutted against one another. Along its dorsolingual surface, the processus posterior bears a shallow, triangular facet for contact with the quadratojugal. This indicates the maxillary arcade was closed posteriorly, forming a bony 'cheek' braced against the

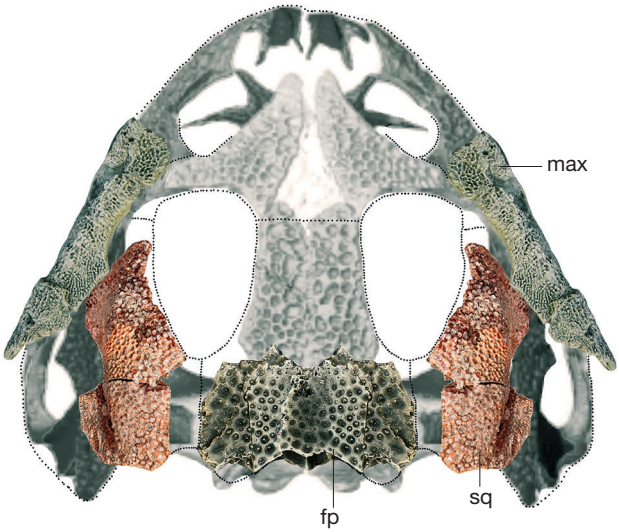

Fig. 7. — Tentative skull reconstruction, in dorsal view, for *Hungarobatrachus szukacsi* Szentesi & Venczel, 2010. Photographs of the fused and anteriorly incomplete frontoparietals (MTM VER 2016.2546), the largest and one of the most nearly complete squamosals (MTM VER 2016.695, left squamosal), and the most nearly complete maxilla (MTM VER 2016.690, right maxilla) are overlain onto skull image of the Eocene anuran *Thaumastosaurus gezei* (modified from Laloy *et al.* 2013: fig. 3A). To improve symmetry, for the frontoparietals the intact portion from its left side was mirrored onto the right side and the left squamosal and right maxilla were mirrored onto the opposite sides of the skull. Dotted lines denote skull outline, inferred natural margins along broken surfaces for bones, and inferred contacts among bones. Although the posterior end of the maxilla is depicted as free, a shallow facet preserved on the dorsolingual surface of MTM VER 2016.690 indicates the maxilla posteriorly contacted the quadratojugal to form a closed 'cheek'. All fossil bones are depicted at their actual sizes relative to one another (i.e., they have not been arbitrarily re-sized in an attempt to improve proportions and contacts). *Thaumastosaurus* De Stefano, 1903 was chosen as the basis for our reconstruction, not because it is closely related (see our phylogenetic analysis and Fig. 8), but because its shape and proportions are a good fit for the available fossil bones of *Hungarobatrachus*. Abbreviations: **fp**, frontoparietals; **max**, maxilla; **sq**, squamosal.

suspensorium. Although none of the available maxillae preserves an intact crista dentalis or any teeth, it is evident that the crista dentalis was shallow. Several specimens (Fig. 5B, F, G, I, L) preserve faint tooth slots along the lingual surface of the crista dentalis that indicate teeth were present, small, closely spaced, and numerous, and that the tooth row terminated posteriorly approximately in line with the base of the processus pterygoideus.

Angulosplenial (Fig. 6)

The posterior portions of two left angulosplenials are available. The less nearly complete specimen, MTM VER 2015.153 (Fig. 6A-C), lacks the posterior end of the extremitas spatulata (= pars spatulaeformis prearticularis), but the preserved bone is uncrushed and has pristine surfaces. Breakage through the posterior portion of the extremitas spatulata in MTM VER 2015.153 reveals small canals extending anteroposteriorly through that portion of the bone (Fig. 6C). The more nearly complete specimen, MTM VER 2016.1948 (Fig. 6D-F) preserves the entire processus coronoideus (= coronoid process) and extremitas spatulata, but exhibits some crushing, the latter being especially evident in the partial closure of the sulcus pro cartilage Meckeli (= Meckelian groove).

The preserved portions of the angulosplenials are typical for anurans in the following features: bone is elongate and sinuosus in dorsal or ventral outline; consisting anteriorly of a rod-like extremitas cultellata (for which only the posteriormost portion is preserved in MTM VER 2016.1948) and posteriorly of an extremitas spatulata, the latter being expanded into a scoop-like structure with its basin opening dorsolabially; the dorsal portion of extremitas spatulata is expanded into an elongate bony flange called the processus coronoideus; the dorsal surface of the processus coronoideus bears a low and broadly convex dorsal tubercle (marked by arrow in Fig. 6A); a low bony ridge called the crista paracoronoidea extends along the dorsolabial surface of the processus coronoideus; and a trough-like sulcus pro cartilage Meckeli extends posteriorly along the labial surface of the extremitas cultellata, widens and ascends dorsally along the processus coronoideus, and ultimately opens into the basin of the extremitas spatulata. The anterior and posterior portions of the processus coronoideus are developed as dorsally convex mounds. Although these mounds are reminiscent of the double coronoid processes in the Oligocene-Recent alytid *Latonia* von Meyer, 1843 (e.g., Roček 1994: fig. 12 and references therein; Biton *et al.* 2013: fig. 3a; Syromyatnikova & Roček 2018: fig. 3), we do not regard them as being homologous, because the mounds in *Hungarobatrachus* are part of an anteroposteriorly elongate and broad, ridge-like processus coronoideus and both are labiolingually broad, relatively low, and subequal in height (versus double coronoid processes in *Latonia* are separate, labiolingually narrow, and relatively taller, with the more posterior process typically being substantially taller and having a more triangular or recurved outline). The lingual surface of the extremitas spatulata in MTM VER 2015.153 is faintly ornamented with tiny pits and low, narrow, anteroposteriorly elongate ridges.

DISCUSSION

Association of newly referred material and distinctiveness of *Hungarobatrachus szukacsi*

When originally described by Szentesi & Venczel (2010), the holotype ilium and referred ilia and tibiofibulae of *Hungarobatrachus szukacsi* were associated using three lines of evidence: 1) the holotype and referred ilia exhibited the same distinctive dorsal crest and interiliac tubercle; 2) size and degree of ossification of the ilia and tibiofibulae indicated they were from similarly-sized individuals; and 3) all specimens came from the same locality and, at that time, no other anurans were known from Iharkút. For the most part, these same three lines of evidence support associating all of the *Hungarobatrachus* specimens reported here: 1) the two new ilia exhibit the same distinctive dorsal crest and interiliac tubercle seen on previously reported ilia; 2) sizes and degree of ossification of the new ilia and skull bones indicate those specimens come from mature individuals of similar size; and 3) the entire collection of ilia, tibiofibulae, and skull bones all come from the same SZÁL-6 site within the Iharkút vertebrate

locality. The newly reported frontoparietals, squamosals, and maxillae can be associated further on the strength of a suite of features indicative of moderate cranial hyperossification, including similar external ornament (exostosis) on all three elements, medial fusion of the frontoparietals, expansion of the frontoparietal posterolaterally to form a broad squamosal process, and expansion of the squamosal to form a broad, plate-like lamella alaris. The newly recognized maxillae and angulosplenials of *Hungarobatrachus* also differ structurally (see next paragraph) from homologous elements previously assigned to the other named frog taxon from Iharkút. Among specimens now available for *Hungarobatrachus*, variation is evident in several features – most notably patterns of ornament on the lateral surface of the dorsal crest on the ilia and on the external surfaces of the squamosals and maxillae – but those differences are relatively minor and we do not regard those as indicating more than one species of *Hungarobatrachus* is represented at Iharkút.

Since *Hungarobatrachus* was named, a second anuran taxon – the alytid *Bakonybatrachus fedori* Szentesi & Venczel, 2012 – has been described from the same site (SZÁL-6) at Iharkút on the basis of the incomplete holotype ilium and fragmentary, single examples of a maxilla, angulosplenial, and scapula. *Bakonybatrachus* Szentesi & Venczel, 2012 differs from *Hungarobatrachus* in being considerably smaller (estimated SVL of just 25-30 mm vs 50-80 mm). Homologous elements of these two sympatric species also differ. Most notably, in *Bakonybatrachus* the ilium lacks an interiliac tubercle and bears only a low and unornamented dorsal crest, the maxilla has a smooth (i.e., unornamented) labial surface and its lamina horizontalis is relatively broader lingually, and the processus coronoideus on the angulosplenial is relatively thinner labiolingually and bears a relatively taller and more triangular dorsal tubercle (see Szentesi & Venczel 2012b: figs 1, 2). Although a *Bakonybatrachus*-like ilium since has been identified from the early Maastrichtian of Romania (Venczel *et al.* 2016), as yet there is no evidence for *Hungarobatrachus* outside of its Santonian type locality at Iharkút.

Hungarobatrachus szukacsi originally was diagnosed largely on the basis of its distinctive ilia. As reported previously by Szentesi & Venczel (2010), the ilia of *Hungarobatrachus* exhibit at least two putative autapomorphies: 1) an extremely high and mediolaterally thick dorsal crest that laterally bears distinctive ridge-and-groove ornament that extends downwards onto the dorsolateral surface of the ilial shaft and 2) an enlarged interiliac tubercle that covers the entire medial surface of the acetabular body, including the preacetabular region, and its medial surface is variably roughened for firm sutural contact with the opposite ilium. Additional ilia and the newly recognized skull bones (frontoparietals, squamosals, maxillae, and angulosplenials) reported here further support the distinctiveness of the species. The unique combination of features presented in our emended diagnosis reliably differentiates *Hungarobatrachus* from all other named extant and extinct anurans, particularly those reported from the Late Cretaceous of Europe (e.g., see summaries by Sanchiz 1998; Roček 2000; Szentesi *et al.* 2013; Venczel *et al.* 2016). Ilial features remain of paramount importance, because that element is so distinctive for *Hungarobatrachus* and ilia are among the most commonly recovered anuran bones at many fossil localities. When compared to slightly younger Maastrichtian-age anurans currently recognized from nearby Romania (see recent review by Venczel *et al.* 2016), the ilium of *Hungarobatrachus* is distinct in the following attributes: 1) dorsal crest present, versus absent in the bombinatorid *Hatzegobatrachus grigorescui* Venczel & Csiki, 2003 (e.g., Venczel & Csiki 2003: figs 1A, 2; Venczel *et al.* 2016: figs 7i-o), but present in other Romanian Maastrichtian anurans; 2) dorsal crest extremely tall and thick, versus crest substantially lower (i.e., less than half the height of the shaft) and thinner in the alytids *Paralatonia transylvanica* Venczel & Csiki, 2003 (e.g., Venczel & Csiki 2003: figs 1B, 3A, C D; Venczel *et al.* 2016: figs 5i-k, 6 a-h), cf. *Bakonybatrachus* sp. (e.g., Venczel *et al.* 2016: fig. 6i, j), and cf. *Eodiscoglossus* sp. (e.g., Folie & Codrea 2005: fig. 3A); 3) lateral face of dorsal crest and adjacent dorsolateral surface of shaft ornamented with pronounced ridges and grooves (versus ornament absent in *Paralatonia* Venczel & Csiki, 2003 and cf. *Eodiscoglossus* sp., but at least one ridge confined to dorsal crest in cf. *Bakonybatrachus* sp.; 4) dorsal protuberance a medially thickened, low, and laterally projecting flange along posterior edge of dorsal crest, versus not a laterally projecting flange in any Romanian Maastrichtian anurans, but instead present either as a low ridge along posterior end of dorsal crest in *Paralatonia*, cf. *Bakonybatrachus* sp., and cf. *Eodiscoglossus* sp. or as a separate, tall ridge with an angular outline and positioned farther back above the acetabulum in *Hatzegobatrachus*; and 5) interiliac tubercle extensive, versus weakly developed in *Paralatonia* and presumably similar in cf. *Bakonybatrachus* sp. and cf. *Eodiscoglossus* sp., but extensively developed in *Hatzegobatrachus*. At a more regional level, for other anurans reported from the Campanian-Maastrichtian of Spain (e.g., Duffaud & Rage 1999; Blain *et al.* 2010; Blanco *et al.* 2016; Szentesi & Company 2017), features such as the lack of a dorsal crest on palaeobatrachid ilia or the presence of a low and unornamented crest in alytid, discoglossid sensu lato, and indeterminate anuran ilia clearly differentiate all of those from *Hungarobatrachus*.

Affinities and paleobiogeographic significance of *Hungarobatrachus szukacsi*

In their type description for the species, Szentesi & Venczel (2010) interpreted *Hungarobatrachus szukacsi* as a neobatrachian and possible ranoid on the basis of two ilial features, namely its high dorsal crest and slender ilioischiadic junction. According to that view, *Hungarobatrachus* was phylogenetically and biogeographically significant for providing a minimum age of Santonian for the establishment of neobatrachians and, potentially, ranoids or ranoid-like anurans in Europe. The skull material reported herein for *Hungarobatrachus* provides an opportunity to assess its affinities by including it, for the first time, in a cladistic analysis.

Our cladistic analysis relies on a modified version of the character-taxon matrix (CTM) employed by Evans *et al.* (2008). Their matrix was adapted from a CTM initially assembled by

Fabrezi (2006) to assess relationships among extant ceratophryids. The Evans *et al.* (2008) CTM retained the same characters, but differed in consolidating some taxa (i.e., combining some congeners into genus) and adding additional taxa, including extinct ones. The Evans *et al.* (2008) CTM is appropriate for assessing relationships of the moderately hyperossified *Hungarobatrachus szukacsi*, because that CTM and its variants have proved informative for assessing relationships across a broad spectrum of extant and extinct hyperossified anurans (e.g., Evans *et al.* 2008, 2014; Báez *et al.* 2009; Laloy *et al.* 2013; Nicoli *et al.* 2016; Báez & Gómez 2018).

The Evans *et al.* (2008) CTM consisted of 67 taxa (genera and species) and 81 osteological and non-osteological characters. For our analysis, we retained the 81 characters and the seven outgroups (bombinatorid *Bombina* Oken, 1816; pipids *Xenopus* Wagler, 1827 and *Hymenochirus* Boulenger, 1896; and pelobatoids *Megophrys* Kuhl & van Hasselt, 1822, *Pelobates* Wagler, 1830, *Spea* Cope, 1866, and *Scaphiopus* Holbrook, 1836). We also made the following changes: 1) reduced the number of taxa to 36 (including the addition of *Hungarobatrachus szukacsi*) to make our analysis more manageable; 2) updated character state scores for the Eocene *Thaumastosaurus*, based on Laloy *et al.*'s (2013) microCT study of a 'mummified', incomplete skeleton of *T. gezei* Rage & Roček, 2007 (see Appendix 1); and 3) updated character state scores for the Maastrichtian *Belzeebufo ampinga* Evans, Jones & Krause, 2008, based on Evans *et al.*'s (2014) description of additional material for that species (see Appendix 1). For *Hungarobatrachus*, we were able to score 11 characters (nine cranial, one ilial, and one size-related), representing 13% of the total character list. For our character list and CTM, see Appendices 1 and 2, respectively. We performed a parsimony analysis using TNT version 1.1 of Goloboff *et al.* (2008), in which the CTM was analysed with the 'New Technology search' option using sectorial search, tree drift, and tree fusing options, all with default parameters.

Our analysis returned four most parsimonious trees of 364 steps, from a total of 2 205 696 rearrangements examined, with the following values: consistency index = 0.327; retention index = 0.554; and homoplasy index = 0.673. Our strict consensus tree (Fig. 8) recovers Neobatrachia as a monophyletic clade, containing a near monophyletic Ranoides (but excluding the microhylid *Callulops* Boulenger, 1888) and a paraphyletic assemblage of *Callulops* and taxa generally regarded as australobatrachian and nobleobatrachian hyloids. In contrast to our expectation that *Hungarobatrachus* was a ranoid, our analysis instead places it within the paraphyletic hyloid and *Callulops* assemblage, where *Hungarobatrachus* is nested within an unnamed clade of hyperossified hyloids containing the hylid *Osteopilus* Fitzinger, 1843, the calyptocephalellid *Calyptocephalella* Strand, 1928, the hemiphractid *Hemiphractus* Wagler, 1828, the ceratophryids *Ceratophrys* Wied-Neuwied, 1824, *Chacophrys* Reig & Limeses, 1963, and *Lepidobatrachus* Budgett, 1899, and the putative ceratophryid *Beelzebufo* Evans, Jones & Krause, 2008. Synapomorphies supporting *Hungarobatrachus* within that unnamed clade are as follows: 8(1) parieto-squamosal arch present (all trees) and, for most trees, 2(1) cranial exostosis present, 6(1) supraorbital alae present, and 11(2) elongate zygomatic ramus of squamosal reaches maxilla. Within the hyperossified hyloid clade, *Hemiphractus* and the ceratophryids form one clade, whereas *Osteopilus*, *Hungarobatrachus*, and *Calyptocephalella* form another. The clade of *Osteopilus* (*Calyptocephalella* + *Hungarobatrachus*) is supported on all four trees by two phalangeal character states (61(1) distal tip of terminal phalanx of toe IV pointed and 68(1) distal tip of terminal phalanx of finger IV pointed) and, on some trees, by another two synapomorphies (13(0) concave anterior end of maxilla and 80(2) noticeable peramorphic traits related to size); of those four synapomorphies, only the last can be scored for *Hungarobatrachus*. The sister pair of *Calyptocephalella* + *Hungarobatrachus* is supported in all four trees by 52(1) ilial crest present.

The results of our cladistic analysis deserve to be treated cautiously, for at least five reasons. First, over 85% of the characters cannot be scored for *Hungarobatrachus*. Second, most of the characters (nine of 11) that can be scored for *Hungarobatrachus* are from the skull. As various authors have noted (e.g., Ruane *et al.* 2011; Báez & Gómez 2014, 2018; Evans *et al.* 2014) the suite of features associated with hyperossification in anurans, such as *Hungarobatrachus,* may bias morphological analyses by artificially grouping those taxa together. Third, all of the synapomorphies supporting the placement of *Hungarobatrachus* within successively less inclusive clades within the Neobatrachia are more widely distributed among anurans (i.e., none is unambiguous for any of the recovered clades). Fourth, most of the recovered clades have weak support. Fifth, some widely accepted neobatrachian clades (e.g., Ranoides) are not fully recovered. Despite those concerns, our analysis appears informative for making some general inferences about the suprafamilial-level affinities of *Hungarobatrachus*. The consistent placement in all four trees of *Hungarobatrachus* nested within an assemblage of taxa generally regarded as hyloids is consistent with earlier interpretations (Szentesi & Venczel 2010; Báez *et al.* 2012; Marjanović & Laurin 2014) that *Hungarobatrachus* is a neobatrachian, but suggests it is more closely related to hyloids rather than ranoids (contra Szentesi & Venczel 2010; Marjanović & Laurin 2014).

The earlier suggestion that *Hungarobatrachus* might be a ranoid was appealing on paleobiogeographic grounds, because at that time Africa was regarded as the continent of origin for ranoids (e.g., Savage 1973; Feller & Hedges 1998; Biju & Bossuyt 2003) and the oldest putative ranoids from Africa (see recent review by Gardner & Rage 2016) were isolated bones from the Cenomanian of Sudan (Báez & Werner 1996) and the Coniacan-Santonian of Niger (Báez & Rage 2004). Szentesi & Venczel (2010) proposed that the ancestor of *Hungarobatrachus* dispersed from Africa, across the proto-Mediterranean, and into southern Europe during the Cenomanian-Santonian interval.

Hyloid affinities for *Hungarobatrachus* do not significantly alter the above scenario. Hyloids also are thought to have originated in Gondwana, probably in the eastern portion consisting of present-day South America, Antarctica, Australia, and New Guinea (e.g., Savage 1973; Feller & Hedges 1998;

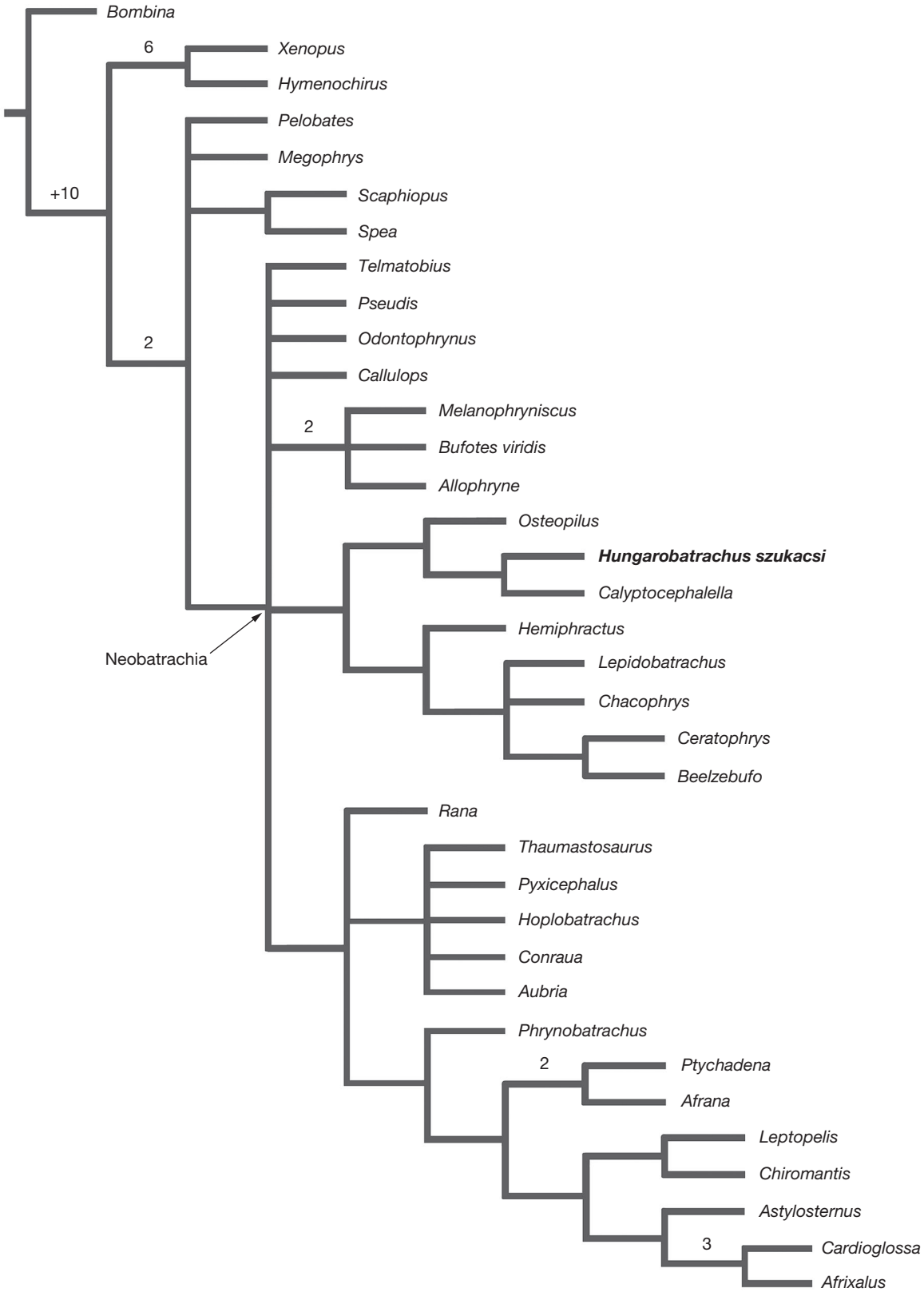

FIG. 8. — Strict consensus of four equally parsimonious trees, recovering *Hungarobatrachus szukacsi* Szentesi & Venczel, 2010 as a neobatrachian, nested within a paraphyletic Hyloides and as sister taxon to the South American Paleogene-Recent genus *Calyptocephalella*. Arabic numbers at nodes denote Bremer support (= decay indices).

San Mauro *et al.* 2005; Bossuyt & Roelants 2009; Pyron 2014; Frazão *et al.* 2015; Streicher *et al.* 2018), during the Late Jurassic-Early Cretaceous (e.g., Feller & Hedges 1998; San Mauro *et al.* 2005; Roelants *et al.* 2007; Wiens 2007; Bossuyt & Roelants 2009; Irisarri *et al.* 2012; Zhang *et al.* 2013; Marjanović & Laurin 2014; Pyron 2014; Hedges *et al.* 2015; Frazão *et al.* 2015; Feng *et al.* 2017). The earliest hyloid or hyloid-like fossils and taxa date from the late Early Cretaceous (Aptian-Albian) of South America (Báez *et al.* 2009). Two occurrences suggest that hyloids were on, or adjacent to, the African continent by the Late Cretaceous. The older, and less certain, occurrence is from the Cenomanian of Morocco, where non-pipoid bones described by Rage & Dutheil (2008) were re-interpreted by Agnolin (2012) as possibly being from a calyptocephalellid. More certain is *Belzeebufo* from the Maastrichtian of Madagascar, which has been regarded variously as a ceratophryid (Evans *et al.* 2008, 2014), a calyptocephalellid (Agnolin 2012), or a hyloid outside of either of those families (Ruane *et al.* 2011; Báez & Gómez 2018).

The sister pairing recovered in our analysis of *Hungarobatrachus* and the South American *Calyptocephalella* is intriguing, although it may simply reflect that both taxa have hyperossified skulls and ilia bearing dorsal crests. *Calyptocephalella* and the more inclusive Calyptocephalellidae generally are regarded as basal hyloids and with an estimated origin in the Early-Late Cretaceous (e.g., San Mauro *et al.* 2005; Frost *et al.* 2006; Roelants *et al.* 2007; Wiens 2007; Bossuyt & Roelants 2009; Pyron & Wiens 2011; Irisarri *et al.* 2012; Marjanović & Laurin 2014; Pyron 2014; Hedges *et al.* 2015; Frazão *et al.* 2015; Feng *et al.* 2017; AmphibiaWeb 2019). The fossil record for calyptocephalellids dates back to the Campanian-Maastrichtian in southern South America (e.g., Agnolin 2012; Nicoli *et al.* 2016: supplemental file F3; Báez & Gómez 2018) and, as mentioned above, the family might also have been present in Africa during the Late Cretaceous.

Assuming that *Hungarobatrachus* is a hyloid, its ancestors still could have dispersed during the Cenomanian-Santonian, across the proto-Mediterranean, from Africa into Europe, as originally suggested by Szentesi & Venczel (2010). There are no other Late Cretaceous records for hyloids in Europe (e.g., see summaries by Sanchiz 1998; Roček 2000; Szentesi *et al.* 2013; Venczel *et al.* 2016). The geologically next youngest European records for neobatrachians and hyloids date from the late Paleocene of Cernay, France, where isolated examples of an indeterminate neobatrachian humerus, radioulna, and vertebra (Estes *et al.* 1967) and two bufonid ilia and a possible bufonid pterygoid (Rage 2003) have been reported.

A recent development may challenge the status of *Hungarobatrachus* as the geologically oldest European neobatrachian. From a new upper Turonian locality in Austria, Ősi *et al.* (2019) reported an incomplete anuran maxilla and vertebrae reminiscent of the Eocene ranoid *Thaumastosaurus*. If those identifications are upheld, the Austrian fossils indicate neobatrachians and ranoids were established in Europe by at least the Turonian, perhaps 5 million years (according to the time scale of Ogg *et al.* 2016) before the appearance of *Hungarobatrachus* in Hungary.

CONCLUSIONS

New ilia and the first skull bones (frontoparietals, squamosals, maxillae, and angulosplenials) from the Upper Cretaceous (Santonian) type locality at Iharkút, Hungary, confirm the distinctiveness of the anuran *Hungarobatrachus szukacsi* Szentesi & Venczel, 2010. Skull features help corroborate the earlier suggestion that *Hungarobatrachus* is a neobatrachian, but argue that instead of being a ranoid as originally suggested based solely on ilial features, *Hungarobatrachus* is a hyloid. *Hungarobatrachus* documents an early record for neobatrachians and hyloids on the present-day European continent, although as suggested by fossils recently reported from the Turonian of Austria, neobatrachians may have a deeper history on the continent than previously suspected. Future work in Upper Cretaceous deposits in Europe and adjacent regions undoubtedly will result in discoveries of additional anuran fossils and taxa that will challenge and refine our understanding of the evolutionary history of anurans on the continent.

Acknowledgements
We are grateful to Atilla Ősi (Eötvös Loránd University, Department of Paleontology, MTA-ELTE Lendület Dinosaur Research Group and Hungarian Natural History Museum, Budapest) for overseeing collecting operations at Iharkút and for his ongoing support of our work on amphibian fossils from that locality and to Krisztina Buczkó (Department of Botany, Hungarian Natural History Museum, Budapest), Réka Kalmár, Gábor Botfalvai, and Márton Szabó (all MTA-ELTE-Lendület Dinosaur Research Group, Budapest, Hungary), and László Makádi (Department of Geological and Geophysical Collections, Mining and Geological Survey of Hungary, Budapest) for their technical support. We thank Hugues-Alexandre Blain (Institut català de Paleoecologia Humana i Evolució Social, Tarragona, Spain) and Elena V. Syromyatnikova (Borissiak Paleontological Institute of the Russian Academy of Sciences, Moscow) for their reviews and Emmanuel Côtez and Sébastien Steyer (both Muséum national d'Historie naturelle, Paris, France) for their editorial assistance. Jean-Claude Rage was a generous and supportive colleague, and we are pleased to have our paper included in this commemorative volume honoring him.

REFERENCES

Agnolin F. 2012. — A new Calyptocephalellidae (Anura, Neobatrachia) from the Upper Cretaceous of Patagonia, Argentina, with comments on its systematic position. *Studia Geologica Salmanticensia* 48: 129-178.

AmphibiaWeb 2019. — Information on amphibian biology and conservation. University of California, Berkeley, CA, USA. Available at: https://amphibiaweb.org [Accessed 31 August 2019.]

Báez A. M. 1987. — The Late Cretaceous fauna of Los Alamitos, Patagonia, Argentina. Part III – Anurans. *Revista del Museo Argentino de Ciencas Naturales 'Bernardino Rivadavia' – Paleontología* 3: 121-130.

BÁEZ A. M. & GÓMEZ R. 2014. — Is hyperossification concealing the phylogenetic signal of osteological traits in Anurans? A test case from the Upper Cretaceous of Brazil. *Society of Vertebrate Paleontology 74th Annual Meeting, Meeting Program & Abstracts, Berlin*: 83.

BÁEZ A. M. & GÓMEZ R. O. 2018. — Dealing with homoplasy: osteology and phylogenetic relationships of the bizarre neobatrachian frog *Baurubatrachus pricei* from the Upper Cretaceous of Brazil. *Journal of Systematic Palaeontology* 16: 279-308. https://doi.org/10.1080/14772019.2017.1287130

BÁEZ A. M. & RAGE J.-C. 2004. — Pipid frogs from the Upper Cretaceous of In Beceten, Niger. *Palaeontology* 41: 669-691.

BÁEZ A. M. & WERNER C. 1996. — Presencia de anuros Ranoideos en el Cretácico de Sudan. *Ameghiniana* 33: 460.

BÁEZ A. M., MOURA G. J. B. & GÓMEZ R. O. 2009. — Anurans from the Lower Cretaceous Crato Formation of northeastern Brazil: implications for the early divergence of neobatrachians. *Cretaceous Research* 30: 829-846. https://doi.org/10.1016/j.cretres.2009.01.002

BÁEZ A. M., GÓMEZ R. O., RIBEIRO L. C. B., MARTINELLI A. G., TEIXEIRA V. P. A. & FERRAZ M. L. F. 2012. — The diverse Cretaceous neobatrachian fauna of South America: *Uberabatrachus carvalhoi*, a new frog from the Maastrichtian Marília Formation, Minas Gerais, Brazil. *Gondwana Research* 22: 1141-1150. https://doi.org/10.1016/j.gr.2012.02.021

BIJU S. D. & BOSSUYT F. 2003. — New frog from India reveals an ancient biogeographical link with the Seychelles. *Nature* 425: 711-*714*. https://doi.org/10.1038/nature02019

BITON R., GEFFEN E., VENCES M., COHEN O., BAILON S., RABINOVICH R., MALKA Y., ORON T., BOISTEL R., BRUMFELD V. & GAFNY S. 2013. — The rediscovered Hula painted frog is a living fossil. *Nature Communications* 4 (1959): 1-6. https://doi.org/10.1038/ncomms2959

BLACKBURN D. C. & WAKE D. B. 2011. — Class Amphibia Gray, 1825, *in* ZHANG Z.-Q. (ed.), Animal biodiversity: An outline of higher-level classification and survey of taxonomic richness. *Zootaxa* 3148: 39-55. https://doi.org/10.11646/zootaxa.3148.1.8

BLAIN H.-A., CANUDO J.-I., CUENCA-BESCÓS G. & LÓPEZ-MARTÍNEZ N. 2010. — Amphibians and squamate reptiles from the latest Maastrichtian (Upper Cretaceous) of Blasi 2 (Huesca, Spain). *Cretaceous Research* 31: 433-446. https://doi.org/10.1016/j.cretres.2010.06.001

BLANCO A., BOLET A., BLAIN H.-A., FONDEVILLA V. & MARMI J. 2016. — Late Cretaceous (Maastrichtian) amphibians and squamates from northeastern Iberia. *Cretaceous Research* 57: 624-638. https://doi.org/10.1016/j.cretres.2015.07.005

BOLKAY S. J. 1919. — Osnove uporedne osteologije anurskih batrahija. *Glasnik Zemaljskog Muzeja u Bosni i Hercegovini* 31: 277-356.

BOSSUYT F. & ROELANTS K. 2009. — Anura, *in* HEDGES S. B. & KUMAR S. (eds), *The Timetree of Life*. Oxford University Press, New York: 357-364.

BOTFALVAI G., HAAS J., BODOR E. R., MINDSZENTY A. & ŐSI A. 2016. — Facies architecture and palaeoenvironmental implications of the upper Cretaceous (Santonian) Csehbánya formation at the Iharkút vertebrate locality (Bakony Mountains, Northwestern Hungary). *Palaeogeography, Palaeoclimatology, Palaeoecology* 441: 659-678. https://doi.org/10.1016/j.palaeo.2015.10.018

CARVALHO A. B., ZAHER H. & NAVA W. R. 2003. — A new anuran Lissamphibia: Tetrapoda) from the continental Late Cretaceous Bauru Basin, State of São Paulo. *XVIII Congresso Brasileiro de Paleontologia, Brasília, Boletim de Resumos*: 188.

CSONTOS L. & VÖRÖS A. 2004. — Mesozoic plate tectonic reconstruction of the Carpathian region. *Palaeogeography, Palaeoclimatology, Palaeoecology* 210: 1-56. https://doi.org/10.1016/j.palaeo.2004.02.033

DUFFAUD S. & RAGE J.-C. 1999. — Amphibians from the Upper Cretaceous of Laño (Basque Country, Spain). *Estudios del Museo de Ciencias Naturales de Alava*, 14 (Número Especial 1): 111-120.

DULAI A., GASPARIK M., SZENTESI Z. & PÁLFY J. 2018. — First supplement to the catalogue of invertebrate and vertebrate palaeontological type specimens of the Hungarian Natural History Museum: 2008-2018. *Fragmenta Palaeontologica Hungarica* 35: 3-59. https://doi.org/10.17111/FragmPalHung.2017.34.3

ESTEBAN M., CASTANET J. & SANCHIZ B. 1995. — Size inferences based on skeletal fragments of the common European frog *Rana temporaria* L. *Herpetological Journal* 5: 229-235.

ESTES R., HECHT M. & HOFFSTETTER R. 1967. — Paleocene amphibians from Cernay, France. *American Museum Novitates* 2295: 1-25. http://hdl.handle.net/2246/3086

EVANS S. E., JONES M. E. H. & KRAUSE D. W. 2008. — A giant frog with South American affinities from the Late Cretaceous of Madagascar. *Proceedings of the National Academy of Sciences USA* 105: 2951-2956. https://doi.org/10.1073/pnas.0707599105

EVANS S. E., GROENKE J. R., JONES M. E. H., TURNER A. H. & KRAUSE D. W. 2014. — New material of *Beelzebufo*, a hyperossified frog (Amphibia: Anura) from the Late Cretaceous of Madagascar. *PLoS ONE* 9 (1): e87236. https://doi.org/10.1371/journal.pone.0087236

FABREZI M. 2006. — Morphological evolution of Ceratophryinae (Anura, Neobatrachia). *Journal of Zoological Systematics and Evolutionary Research* 44: 153-166. https://doi.org/10.1111/j.1439-0469.2005.00349.x

FELLER A. E. & HEDGES S. B. 1998. — Molecular evidence for the early history of living amphibians. *Molecular Phylogenetics and Evolution* 9: 509-516. https://doi.org/10.1006/mpev.1998.0500

FENG Y.-J., BLACKBURN D. C., LIANG D., HILLIS D. M., WAKE D. B. CANNATELLA D. C. & ZHANG P. 2017. — Phylogenomics reveals rapid, simultaneous diversification of three major clades of Gondwanan frogs at the Cretaceous–Paleogene boundary. *Proceedings of the National Academy of Sciences USA* 114: E5864-E5870. https://doi.org/10.1073/pnas.1704632114

FISCHER G. 1813. — *Zoognosia tabulis synopticis illustrata, in usum praelectionum Academiae Imperialis Medico-Chirurgicae Mosquensis edita*. Vol. 1, 3rd ed. Nicolai Sergeidis Vsevolzsky, Moscow. https://doi.org/10.5962/bhl.title.42225

FOLIE A. & CODREA V. 2005. — New lissamphibians and squamates from the Maastrichtian of Haţeg Basin, Romania. *Acta Palaeontologica Polonica* 50: 57-71.

FRAZÃO A., DA SILVA H. R. & DE MORAES RUSSO C. A. 2015. — The Gondwana breakup and the history of the Atlantic and Indian oceans unveils two new clades for early neobatrachian diversification. *PLoS ONE* 10 (11): e0143926. https://doi.org/10.1371/journal.pone.0143926

FROST D. R. 2019. — Amphibian species of the World: an online reference. Version 6.0 American Museum of Natural History, New York, USA. Available at: http://research.amnh.org/herpetology/amphibia/index.html [accessed 31 August 2019.]

FROST D. R., GRANT T., FAIVOVICH J., BAIN R. H., HAAS A., HADDAD C. F. B., DE SÁ R. O., CHANNING A., WILKINSON M., DONNELLAN S. C., RAXWORTHY C. J., CAMPBELL J. A., BLOTTO B. L., MOLER P. E., DREWES R. C., NUSSBAUM R. A., LYNCH J. D., GREEN D. M. & WHEELER, W. C. 2006. — The amphibian tree of life. *Bulletin of the American Museum of Natural History* 297: 1-370. https://doi.org/d7tmxr

GARDNER J. D. & RAGE J.-C. 2016. — The fossil record of lissamphibians from Africa, Madagascar, and the Arabian Plate. *Palaeobiodiversity and Palaeoenvironments* 96: 169-220. https://doi.org/10.1007/s12549-015-0221-0

GOLOBOFF P. A., FARRIS J. S. & NIXON K. C. 2008. — TNT, a free program for phylogenetic analysis. *Cladistics* 24: 774-786, https://doi.org/10.1111/j.1096-0031.2008.00217.x

GÓMEZ R. O. & TURAZZINI G. F. 2016. — An overview of the ilium of anurans (Lissamphibia, Salientia), with a critical appraisal of the terminology and primary homology of main ilial features. *Journal of Vertebrate Paleontology*: e1030023. https://doi.org/10.1080/02724634.2015.1030023

Hedges S. B., Marin J., Suleski M., Paymer M. & Kunar S. 2015. — Tree of life reveals clock-like speciation and diversification. *Molecular Biology and Evolution* 32: 835-845. https://doi.org/10.1093/molbev/msv037

Irisarri I., San Mauro D., Abascal F., Ohler A., Vences M. & Zardoya, R. 2012. — The origin of modern frogs (Neobatrachia) was accompanied by acceleration in mitochondrial and nuclear substitution rates. *BMC Genomics* 13: 626. https://doi.org/10.1186/1471-2164-13-626

Laloy F., Rage J.-C., Evans S. E., Boistel R., Lenoir N. & Laurin, M. 2013. — A reinterpretation of the Eocene anuran *Thaumastosaurus* based on microCT examination of a 'mummified' specimen. *PLoS ONE* 8 (9): e74874. https://doi.org/10.1371/journal.pone.0074874

Lynch J. D. 1971. — Evolutionary relationships, osteology, and zoogeography of leptodactyloid frogs. *University of Kansas Museum of Natural History Miscellaneous Publication* 53: 1-238. https://www.biodiversitylibrary.org/page/3662221

Marjanović D. & Laurin M. 2014. — An updated paleontological timetree of lissamphibians, with comments on the anatomy of Jurassic crown-group salamanders (Urodela). *Historical Biology* 26: 535-550. https://doi.org/10.1080/08912963.2013.797972

Nicoli L., Muzzopappa P. & Faivovich J. 2016. — The taxonomic placement of the Miocene frog *Wawelia gerholdi* (Amphibia: Anura). *Alcheringa* 40: 153-160. https://doi.org/10.1080/03115518.2016.1101998

Noble G. K. 1930. — The fossil frogs of the intertrappean beds of Bombay, India. *American Museum Novitates* 401: 1-13. http://hdl.handle.net/2246/3061

Ogg J. G., Ogg G. M. & Gradstein F. M. 2016. — *A Concise Geologic Time Scale 2016*. Elsevier, Amsterdam.

Ősi A. & Mindszenty A. 2009. — Iharkút, Dinosaur-bearing alluvial complex of the Csehbánya Formation, *in* Babinszky E. (ed.), *Cretaceous Sediments of the Transdanubian Range. Field Guide of the Geological Excursion Organized by the Sedimentological Subcommission of the Hungarian Academy of Sciences and the Hungarian Geological Society*. MÁFI, Budapest: 51-63. http://real.mtak.hu/id/eprint/84473

Ősi A., Makádi L., Rabi M., Szentesi Z., Botfalvai G. & Gulyás P. 2012. — The Late Cretaceous continental vertebrate fauna from Iharkút, western Hungary: a review, *in* Godefroit P. (ed.), *Bernissart Dinosaurs and Early Cretaceous Terrestrial Ecosystems*. Indiana University Press, Bloomington: 533-568. https://www.jstor.org/stable/j.ctt16gzfhx.35

Ősi A., Szabó M., Kollmann H., Wagreich M., Kalmár R., Makádi L., Szentesi Z. & Summesberger S. 2019. — Vertebrate remains from the Turonian (Upper Cretaceous) Gosau Group of Gams, Austria. *Cretaceous Research* 99: 190-208. https://doi.org/10.1016/j.cretres.2019.03.001

Prasad G. V. R. & Rage J.-C. 1995. — Amphibians and squamates from the Maastrichtian of Naskal, India. *Cretaceous Research* 16: 95-107. https://doi.org/10.1006/cres.1995.1006

Prasad G. V. R. & Rage J.-C. 2004. — Fossil frogs (Amphibia: Anura) from the Upper Cretaceous intertrappean beds of Naskal, Andhra Pradesh, India. *Revue de Paléobiologie* 23: 99-116.

Pyron R. A. 2014. — Biogeographic analysis reveals ancient continental vicariance and recent oceanic dispersal in amphibians. *Systematic Biology* 63: 779-797. https://doi.org/10.1093/sysbio/syu042

Pyron R. A. & Wiens J. J. 2011. — A large-scale phylogeny of Amphibia including over 2800 species, and a revised classification of extant frogs, salamanders, and caecilians. *Molecular Phylogenetics and Evolution* 61: 543-583. https://doi.org/10.1016/j.ympev.2011.06.012

Rage J.-C. 2003. — Oldest Bufonidae (Amphibia, Anura) from the Old World: a bufonid from the Paleocene of France. *Journal of Vertebrate Paleontology* 23:462-463. https://doi.org/drdzwp

Rage J.-C. & Dutheil D. B. 2008. — Amphibians and squamates from the Cretaceous (Cenomanian) of Morocco. A preliminary study, with description of a new genus of pipid frog. *Palaeontographica Abteilung A* 285: 1-22. https://doi.org/10.1127/pala/285/2008/1

Rage J.-C. & Roček Z. 2007. — A new species of *Thaumastosaurus* (Amphibia: Anura) from the Eocene of Europe. *Journal of Vertebrate Paleontology* 27: 329-336. https://doi.org/c6p9xf

Reig O. A. 1958. — Proposiciones para una nueva macrosistematica de los anuros (Nota preliminar). *Physis* 21: 109-118

Roček Z. 1981. — Cranial anatomy of frogs of the family Pelobatidae Stanius, 1856, with outlines of their phylogeny and systematics. *Acta Universitatis Carolinae – Biologica* 1980: 1-164.

Roček Z. 1994. — Taxonomy and distribution of Tertiary discoglossids (Anura) of the genus *Latonia* v. Meyer, 1843. *Geobios* 27: 717-751. https://doi.org/10.1016/S0016-6995(94)80058-8

Roček Z. 2000. — Mesozoic anurans, *in* Heatwole H. & Carroll R. L. (eds), *Amphibian Biology 4: Palaeontology*. Surrey Beatty & Sons, Chipping Norton: 1295-1331. https://doi.org/bt5drp

Roček Z. 2013. — Mesozoic and Tertiary Anura of Laurasia. *Palaeobiodiversity and Palaeoenvironments* 93: 397-439. https://doi.org/10.1007/s12549-013-0131-y

Roček Z. & Lamaud P. 1995. — *Thaumastosaurus bottii* de Stefano, 1903, an anuran with Gondwanan affinities from the Eocene of Europe. *Journal of Vertebrate Paleontology* 15: 506-515. https://doi.org/10.1080/02724634.1995.10011244

Roelants K., Gower D. J., Wilkinson M., Loader S. P., Biju S. D., Guillaume K., Moriau L. & Bossuyt F. 2007. — Global patterns of diversification in the history of modern amphibians. *Proceedings of the National Academy of Sciences* 104: 887-892. https://doi.org/10.1073/pnas.0608378104

Ruane S., Pyron R. A. & Burbrink F. T. 2011. — Phylogenetic relationships of the Cretaceous frog *Beelzebufo* from Madagascar and the placement of fossil constraints based on temporal and phylogenetic evidence. *Journal of Evolutionary Biology* 24: 274-285. https://doi.org/10.1111/j.1420-9101.2010.02164.x

Sanchiz B. 1998. — Salientia, *in* Wellnhofer P. (ed.), *Encyclopedia of Paleoherpetology.* Part 4. Verlag Dr. Friedrich Pfeil, München, 275 p.

San Mauro D., Vences M., Alcobendas M., Zardoya M. & Meyer A. 2005. — Initial diversification of living amphibians predated the breakup of Pangea. *The American Naturalist* 165: 590-599. https://doi.org/10.1086/429523

Savage J. M. 1973. — The geographical distributions of frogs: patterns and predictions, *in* Vial J. L. (ed.), *Evolutionary Biology of the Anurans. Contemporary Research on Major Problems*. University of Missouri Press, Columbia: 351-445.

Špinar Z. V. & Hodrova M. 1985. — New knowledge of the genus *Indobatrachus* (Anura) from the Lower Eocene of India. *Amphibia-Reptilia* 6: 363-376. https://doi.org/10.1163/156853885X00353

Streicher J. W., Miller E. C., Guerrero P. C., Correa C., Ortiz J. C., Crawford A. J., Pie M. R. & Wiens J. J. 2018. — Evaluating methods for phylogenomic analyses, and a new phylogeny for a major frog clade (Hyloidea) based on 2214 loci. *Molecular Phylogenetics and Evolution* 119: 128-143. https://doi.org/10.1016/j.ympev.2017.10.013

Syromyatnikova E. V. & Roček Z. 2018. — New *Latonia* (Amphibia: Alytidae) from the late Miocene of northern Caucasus (Russia). *Palaeobiodiversity and Palaeoenvironments* 99: 495-509. https://doi.org/10.1007/s12549-018-0350-3

Szabó M., Gulyás P. & Ősi A. 2016. — Late Cretaceous (Santonian) *Atractosteus* (Actinopterygii, Lepisosteidae) remains from Hungary (Iharkút, Bakony Mountains). *Cretaceous Research* 60: 239-252. https://doi.org/10.1016/j.cretres.2015.12.002

Szentesi Z. & Company J. 2017. — Late Maastrichtian small-sized herpetofauna from Valencia province, eastern Spain. *Historical Biology* 29: 43-52. https://doi.org/10.1080/08912963.2015.1122004

SZENTESI Z. & VENCZEL M. 2010. — An advanced anuran from the Late Cretaceous (Santonian) of Hungary. *Neues Jahrbuch für Geologie und Paläontologie, Abhandlungen* 256: 291-302. https://doi.org/10.1127/0077-7749/2010/0054

SZENTESI Z. & VENCZEL M. 2012a. — Egy fejlett béka a késő-kréta (santoni) Csehbányai Formációból (Iharkút, Bakony-hegység) [An advanced anuran from the Late Cretaceous (Santonian) Csehbánya Formation (Iharkút, Bakony Mountains]. *Földtani Közlöny* 142: 33-44.

SZENTESI Z. & VENCZEL M. 2012b. — A new discoglossid frog from the Upper Cretaceous (Santonian) of Hungary. *Cretaceous Research* 34: 327-333. https://doi.org/10.1016/j.cretres.2011.11.012

SZENTESI Z., GARDNER J. D. & VENCZEL M. 2013. — Albanerpetontid amphibians from the Late Cretaceous (Santonian) of Iharkút, Hungary, with remarks on regional differences in Late Cretaceous Laurasian amphibian assemblages. *Canadian Journal of Earth Sciences* 50: 268-281. https://doi.org/10.1139/e2012-024

TRUEB L. 1973. — Bones, frogs, and evolution, *in* VIAL J. L. (ed.), *Evolutionary Biology of the Anurans. Contemporary Research on Major Problems*. University of Missouri Press, Columbia: 65-132.

TRUEB L. 1993. — Patterns of structural diversity among the Lissamphibia, *in* HANKEN J. & HALL B. K. (eds), *The Skull*. Volume 2. *Patterns of Structural and Systematic Diversity*. University of Chicago Press, Chicago: 255-343.

VENCZEL M. & CSIKI Z. 2003. — New frogs from the latest Cretaceous of Haţeg Basin, Romania. *Acta Palaeontologica Polanica* 48: 609-616.

VENCZEL M. & SZENTESI Z. 2012. — Locomotory techniques in Upper Cretaceous frogs (Iharkút, Hungary). *Hantkeniana* 7: 19-25.

VENCZEL M., GARDNER J. D., CODREA V. A., CSIKI-SAVA Z, VASILE Ş. & SOLOMON A. A. 2016. — New insights into Europe's most diverse Late Cretaceous anuran assemblage from the Maastrichtian of western Romania. *Palaeobiodiversity and Palaeoenvironments* 96: 61-95. https://doi.org/10.1007/s12549-015-0228-6

WIENS J. J. 2007. — Global patterns of diversification and species richness in amphibians. *The American Naturalist* 170 (supplement): S86-S106. https://doi.org/10.1086/519396

ZHANG P., LIANG D., MAO R.-L., HILLIS D. M., WAKE D. B. & CANNATELLA, D. C. 2013. — Efficient sequencing of anuran mtDNAs and a mitogenomic exploration of the phylogeny and evolution of frogs. *Molecular Biology and Evolution* 30: 1899-1915. https://doi.org/10.1093/molbev/mst091

Submitted on 12 September 2019;
accepted on 10 December 2019;
published on 8 April 2021.

Appendix 1. — Character-taxon matrix and coding.

The character-taxon matrix (CTM) in our cladistic analysis is based on a modified version of the CTM employed by Evans *et al*. (2008) consisting of 67 anuran taxa (genera and species) and 81 osteological and non-osteological characters. The CTM of Evans *et al*. (2008) has been adapted from a CTM initially assembled by Fabrezi (2006) to assess relationships among extant ceratophryids. Modifications to the CTM and character state scores of Evans *et al*. (2008) include: 1) reduction of the number of anuran taxa to 36 (including the addition of *Hungarobatrachus szukacsi* Szentesi & Venczel, 2010); 2) updates of the character state scores for the Eocene *Thaumastosaurus* De Stefano, 1903, based on Laloy *et al*.'s (2013) microCT study of a 'mummified', incomplete skeleton of *T. gezei* Rage & Roček, 2007: character 1: changed from 0 to 1; character 7: changed from 0 to 1; character 12: changed from [1, 2] to ?; character 14: changed from ? to 0; character 16: changed from 0 to 1; character 19: changed from ? to 2; character 20: changed from ? to 0; character 21: changed from ? to 2; character 23: changed from ? to 0; character 24: changed from ? to 1; character 34: changed from ? to 0; character 35: changed from ? to 1; character 36: changed from ? to 0; character 37: changed from ? to 0; character 38: changed from ? to 0; character 39: changed from ? to 1; character 40: changed from ? to 1; character 41: changed from ? to 0; character 42: changed from ? to 2; character 43: changed from ? to 0; character 44: changed from ? to 0; character 45: changed from ? to 0; character 46: changed from ? to 2; character 47: changed from ? to 2; character 48: changed from ? to 0; character 49: changed from ? to 0; character 50: changed from ? to 3; character 51: changed from ? to 1; character 52: changed from ? to 1; character 80: changed from ? to 2; 3) updates of the character state scores for the Maastrichtian *Belzeebufo ampinga* Evans, Jones & Krause, 2008, based on Evans *et al*.'s (2014) description of additional material for that species: character 13: changed from ? to 2; and character 18: changed from ? to 0.

CHARACTER STATE LIST

Note that the original list of Fabrezi (2006) and Evans *et al*. (2008) began with "0", and we have followed that convention for ease of comparison with those earlier analyses.

0. Nasal shape: 0 – triangular and large; 1 – reduced to a narrow slip of bone;
1. Nasals medial contact: 0 – fused or in contact; 1 – moderately to widely separated;
2. Cranial exostosis: 0 – absent; 1 – present;
3. Dorsal exposure of sphenethmoid: 0 – invisible dorsally; 1 – visible dorsally;
4. Ventral configuration of sphenethmoid: 0 – a single bone; 1 – consisting of two elements;
5. Frontoparietals medial contact: 0 – no medial contact; 1 – slightly separated; 2 – sutured or fused;
6. Supraorbital alae (= tectum supraorbitale) of frontparietal: 0 – absent; 1 – present;
7. Frontoparietals: 0 – parallel sided; 1 – posterior end wider than anterior end;
8. Parieto-squamosal arch: 0 – absent; 1 – present;
9. Interfrontal: 0 – absent; 1 – present;
10. Otic ramus (= ramus paroticus) of squamosal: 0 – absent or rudimentary; 1 – overlapping crista parotica; 2 – overlapping crista parotica and otoccipital;
11. Zygomatic ramus (= processus zygomaticus) of squamosal: 0 – short or absent; 1 – moderately developed; 2 – long, reaching maxilla;
12. Teeth: 0 – absent; 1 – bicuspid; 2 – monocuspid;
13. Shape of anterior end of maxilla: 0 – concave; 1 – straight;
14. Pars palatina (= lamina horizontalis) of premaxilla: 0 – present; 1 – reduced; 2 – absent;
15. Orientation of processus alaris of premaxillae: 0 – parallel; 1 – divergent;
16. Pars facialis of maxilla: 0 – low; 1 – high;
17. Anterior ramus of pterygoid: 0 – long, reaching antorbital planum; 1 – short;
18. Pterygoid rami: 0 – well differentiated; 1 – posterior and medial rami forming a plate;
19. Prevomer: 0 – absent or unpaired; 1 – incomplete, without odontophore; 2 – complete;
20. Anterior process of prevomer: 0 – long, reaching the premaxilla-maxilla articulation; 1 – reduced, not reaching premaxilla-maxilla articulation;
21. Quadratojugal: 0 – absent or reduced; 1 – entire, but not contacting maxilla; 2 – articulated or fused to maxilla;
22. Palatine: 0 – absent; 1 – present;
23. Fangs in lower jaw: 0 – absent; 1 – forming a plate of dentary; 2 – a spur-like projection formed by dentary and mentomeckelian bones;
24. Mentomeckelian bone: 0 – absent; 1 – distinct from dentary; 2 – fused to dentary;
25. Ceratohyalia: 0 – continuous; 1 – discontinuous;
26. Ceratohyalia processes: 0 – absent; 1 – anteromedial processes; 2 – anteromedial and anterolateral processes;
27. Anterolateral process of hyoid plate: 0 – absent; 1 – pointed; 2 – dilated distally; 3 – expanded;
28. Posterolateral process of hyoid plate: 0 – absent; 1 – present;
29. Posteromedial process ossification: 0 – ossification present on a cartilaginous stalk; 1 – ossification abuts directly on the hyoid; 2 – ossification invades the hyoid;
30. Posteromedial epiphyses: 0 – cartilaginous; 1 – ossified;
31. Posteromedial ridge of posteromedial process: 0 – absent; 1 – present;

32. Parahyoid bone: 0 – absent; 1 – small ossification; 2 – transverse bar;
33. Endochondral ossifications in the hyoid: 0 – absent; 1 – present;
34. Number of presacral vertebrae: 0 – eight; 1 – seven;
35. Shape of eighth vertebra: 0 – opisthocoelous; 1 – procoelous; 2 – biconcave;
36. Cervical cotyle arrangement: 0 – contiguous; 1 – separated;
37. Sacral vertebra and urostyle: 0 – articulated; 1 – fused;
38. Eigth presacral and sacral vertebrae: 0 – separated; 1 – fused;
39. Neural arches: 0 – imbricate; 1 – non-imbricate;
40. Neural spines: 0 – low; 1 – high; 2 – flattened;
41. Relative length of transverse processes: 0 – decrease gradually in caudal direction; 1 – decreases abruptly from fourth vertebra in caudal direction;
42. Sacral transverse processes: 0 – widely expanded; 1 – moderately dilated; 2 – cylindrical;
43. Ribs: 0 – absent; 1 – present;
44. Dorsal shields: 0 – absent; 1 – two ossifications; 2 – complex formed by a set of plates;
45. Orientation of transverse processes on eighth presacral vertebra: 0 – perpendicular to axial axis; 1 – markedly forward; 2 – absent;
46. Omosternum: 0 – cartilaginous; 1- ossified, not forked; 2 – ossified, forked; 3 – absent;
47. Metasternum: 0 – absent; 1 – cartilaginous; 2 – proximal ossified style;
48. Coracoid: 0 – entire medial margin; 1 – perforated medial margin;
49. Clavicle: 0 – well developed; 1 – reduced; 2 – absent;
50. Epicoracoid: 0 – widely overlapping; 1 – slightly overlapping; 2 – fused; 3 – absent, coracoids with medial union (firmisterny);
51. Scapula: 0 – short; 1 – long;
52. Dorsal crest on iliac shaft: 0 – absent; 1 – present;
53. Epipubis: 0 – absent; 1 – present;
54. Femoral crest: 0 – absent; 1 – present;
55. Intercalary element: 0 – absent; 1 – present;
56. Tarsal sesamoidea: 0 – absent; 1 – cartilage sesamoidea; 2 – os sesamoidea tarsale;
57. Distal tarsal 3 and distal tarsal 2: 0 – free; 1 – fused;
58. Distal tarsal 1: 0 – absent; 1 – present;
59. Prehallux: 0 – one spherical proximal element; 1 – two elements, the distal one enlarged; 2 – three or more elements; 3 – two elements, the distal one hypermorphic;
60. Shape of terminal phalanx of toe IV: 0 – straight; 1 – curved;
61. Distal tip of terminal phalanx of toe IV: 0 – knob-like; 1 – pointed; 2 – notched; 3 – T-shaped; 4 – Y-shaped;
62. Ventral spine of toe IV: 0 – absent; 1 – present;
63. Subarticular sesamoidea of toes: 0 – absent; 1 – present;
64. Postaxial carpals (ulnare and distals 5 and 4): 0 – unfused; 1 – ulnare free, 5 and 4 fused; 2 – ulnare free, 3, 4 and 5 fused; 3 – ulnare and 5 fused, 4 free;
65. Preaxial carpals (element Y and distal 2): 0 – unfused; 1 – 2 and Y fused; 2 – element Y, distal 2 and 3 fused;
66. Prepollex: 0 – one spherical proximal element; 1 – two elements, the distal one enlarged; 2 – three or more elements; 3 – two elements, the distal one hypermorphic;
67. Shape of terminal phalanx of finger IV: 0 – straight; 1 – curved;
68. Distal tip of terminal phalanx of finger IV: 0 – knob-like; 1 – pointed; 2 – notched; 3 – T-shaped; 4 – Y – shaped;
69. Ventral spine of finger IV: 0 – absent; 1 – present;
70. Subarticular sesamoidea of finger IV: 0 – absent; 1 – present;
71. Carpal torsion: 0 – absent; 1 – present;
72. Parotoid glands: 0 – absent; 1 – present;
73. Bidder organ: 0 – absent; 1 – present;
74. Development: 0 – direct; 1 – larval;
75. Spiracle in larva: 0 – pair; 1 – single and sinistral; 2 – single and medial; 3 – single, medial and posterior;
76. Keratinised jaws in larva: 0 – absent; 1 – present;
77. Keratodonts in larva: 0 – absent; 1 – present;
78. Sexual dimorphism in size: 0 – females larger than males; 1 – females equal or smaller than males;
79. Sexual dimorphism in finger length: 0 – absent; 1 – present;
80. Heterochronic traits related to size: 0 – absent; 1 – noticeable paedomorphic traits; 2 – noticeable peramorphic traits.

Appendix 2. — Matrix of *Hungarobatrachus szukacsi* Szentesi & Venczel, 2010, available here (https://doi.org/10.5852/geodiversitas2021v43a7_s1).